Numerical Investigation on Nanofluid based High Temperature Direct Absorption Solar Collector

A Thesis

Submitted in partial fulfillment of
requirements for the degree of

Master of Engineering

In

Thermal Engineering

By

Ashish Kumar Shukla

Registration No.: 801583005

Under the Supervision of

Dr. Vikrant Khullar

(Assistant Professor, MED)

MECHANICAL ENGINEERING DEPARTMENT

THAPAR UNIVERSITY, PATIALA

July, 2017

CERTIFICATE

I hereby declare that the thesis entitled "**Numerical Investigation on Nanofluid based High Temperature Direct Absorption Solar Collector**" is an authentic record of my work carried out as requirements for the award of the degree of **Master of Engineering** in **Thermal Engineering** at **Thapar University, Patiala** under the supervision of **Dr. Vikrant Khullar** (Assistant Professor, Mechanical Engineering Department, Thapar University) during July, 2015 to July, 2017. No part of the matter embodied in this report has been submitted to any other university or institute for the award of any degree.

Date: 31/07/2017

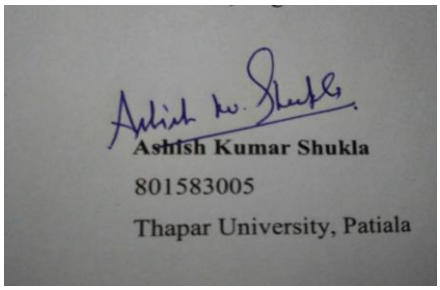

It is certified that the above statement made by the student is correct to the best of our knowledge and belief.

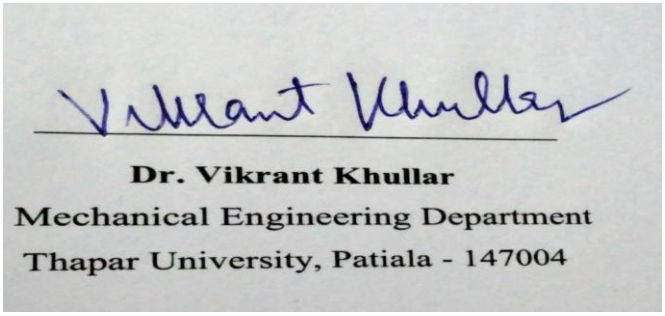

Dedicated to
My parents
And god

Acknowledgements

I would like to thank my supervisor, Dr. Vikrant Khullar, for the patient guidance, encouragement and advice he has provided throughout my time as his student. I have been extremely lucky to have a supervisor who cared so much about my work, and who responded to my questions and queries so promptly.

I would also like to express my deep sense of gratitude to my parents for allowing me to realize my own potential. All the support they have provided me over the years was the greatest gift anyone has ever given me.

The days would have passed far more slowly without the support of my friend, Mr. Rishabh Prakash Sharma, Research Scholar, Department of Mechanical Engineering, Thapar University, Patiala, whom I thank for putting up with my idiosyncrasies and for providing such a rich source of conversation, education and computation.

Finally, I would like to extend my sincere thanks to my dear god, who led me to go through the difficult time of my life with his profound and unconditional love for me.

Ashish Kumar Shukla

Abstract

The advance and efficient solar thermal systems are necessary to remove the burden on fossil fuel energy generation technology. In present work, analysis of nanofluid based volumetric receiver, has been done to evaluate the efficiency of nanofluid based high temperature direct absorption solar collector in which nanoparticles absorb incident solar radiation directly within the fluid. The concept of harvesting solar radiation by direct absorbing nanofluid recently been shown numerically and experimentally to be an efficient method. Dispersing small amount of nanoparticles in heat transfer fluid (HTF) significantly alters the optical as well as thermophysical properties of HTF. This study is to contribute towards the development of volumetric flow receiver design and to quantify the effect of different parameter over the thermal efficiency of the receiver. Furthermore, to quantify the absorption capability, solar weighted absorptivity of copper nanoparticles dispersed in water/ silicon oil have been computed by using DDSCAT Fortran-90 open package software.

For Numerical investigation of receiver, it has been mathematically modeled (two dimensional), and the governing equations, convection-diffusion (C-D) equation and radiative transfer equation (RTE), have been numerically solved using finite difference technique. In order to evaluate the temperature profile inside the receiver and convective and radiative losses from the collector, the energy balance equation, RTE and heat transport equation were solved by using MATLAB software. It was observed that by changing the concentration ratio and bottom wall optical properties, the overall system performance such as thermal efficiency, average outlet temperature and radiative losses alter significantly. Furthermore, Optical properties of nanoparticles closely related to shape, size and the dielectric medium in which the nanoparticles dispersed. As the aspect ratio of nanoparticles and effective diameter varies the absorption and scattering peaks of changes significantly, also solar weighted absorption coefficient increases with volume fraction of the nanoparticles.

Key words: solar energy, direct absorption, nanofluids, thermal efficiency

Table of Contents

List of Figures

List of Tables

Nomenclature

A_S	Surface area, m^2
D	Diameter of nanoparticles, m
V	Velocity, m/s
f	Frictional factor
L_e	Entrance length, m
k	Absorption coefficient , Thermal conductivity
L	Length, m
H	Receiver height
f_v	Volume fraction (%)
V	Volume, m^3
Re	Reynolds number
ΔP	Pressure gradient, (Kpa)
C_p	Specific heat at constant pressure, (J/KgK)
q	heat flux
Q	Discharge, m^3/s
I	Intensity, (W/m^2)
h	convective heat-transfer coefficient, Planck's constant
m	complex refractive index $(n+i\kappa)$, mass flow rate
n	Index of refraction
x,y,z	Cartesian coordinates
u,v,w	Velocity components in Cartesian coordinates
t	Optical thickness

Greek Symbols

μ	direction cosine with respect to y-direction, coefficient of viscosity
ρ	reflectivity; density
α	size parameter, absorptivity
ε	Emissivity
ϕ	azimuthal angle
Ω	Solid angle
τ	transmissivity
Γ	fraction factor
Φ	dissipation function

Subscripts

λ	Spectral wavelength (μm)
n	nanoparticles
g	glass
w	wall
b	base-fluid, black body
a,e,s	Absorption, extinction, scattering
r	radiative
∞	ambient
0	Coordinate origin
in	Inlet
nf	Nanofluids

Acronyms

STS	Solar thermal system
HTF	Heat transfer fluid
DSAS	Direct Solar thermal Absorption system
FDM	Finite Difference Method
CR	Concentration Ratio
MWCNT	Multi walled Carbon Nano-tubs
CNTs	Carbon Nano-tubes
Re	Reynolds number
IEP	Isoelectric point

Chapter 1

Introduction

1. Introduction

1.1. Motivation

Today demand of energy generation to full fill the human need is most of the critical field in research area. The energy generation from non-sustainable natural resources has adverse impact on environmental changes like global warming. From last two decades researcher are working to find the alternative source of energy like from nuclear power, hydro power, biomass, wind energy and solar energy. In all these resources solar energy has least efficient method to convert sun energy to thermal energy. Solar thermal energy harvesting technique is one of the most sensible and effective way of energy generation. These techniques expected to solve the energy crisis without harm to the environment. Existing solar technology are not operating efficiently which leaves the room for improvement for future solar thermal system (STS). In solar thermal systems, one main constituent is the collector receiver, which works as a heat exchanger that converts the solar irradiation intensity to internal energy of the transport medium. Currently, STS are used in both domestic and industrial purpose like electricity generation, water heating, space heating and cooling and desalination.

Demands always force the scientist to provide the improvement in the existing systems, also to make agreements with explore of new possibility. Most of the present solar thermal system is surface based, wherein sun radiation first absorb by solar selective surface and then it transfer to heat transfer fluid (HTF) through conduction and convection mode of heat transfer. For high temperature application they suffers high radiative losses and convective thermal losses is larger resulting in inefficient solar thermal energy conversion from surface which reduces its efficiency to absorb solar irradiation in Fig.2. Solar radiation can be directly absorbed directly by the Heat transfer fluid (HTF) without heating any other material within collector refer as direct solar thermal absorption system (DSAS), in which low convective heat losses possible. The technique of direct absorption of solar irradiation was presented in the 70's as a simplification of conventional collector design to potentially enhance the efficiency by absorbing irradiation within the fluid volume.

This novel concept of were the first to present direct absorption solar receiver using a suspension of micro-sized carbonaceous particles in shellac, known as Indian Ink, as a volumetric receiver (Minard et al., 1974). DSAS technique opens the new class of research to use of materials in the base fluid. At present, most of the STS based on surface based absorption system, where solar irradiation first absorbs by surface (usually coated, as shown in Figure 1.1). Solar selective coating is applied over the absorbing surface in order to enhance absorptivity throughout the incident solar irradiation spectrum and reduce emissivity across thermal radiation spectrum. Absorbing surface always acts as a thermal barrier between HTF and incident flux, which is sensitive at high temperature application, effects of lower thermal efficiency (As shown in Fig.1.2). The objective of this thesis to understand the physically possible phenomena of heat transfer in the volumetric solar receiver with varying parameter like concentration ratio, volume fraction, receiver height and boundary conditions. The efficiency of solar thermal system or high solar to thermal energy conversion depends on effectiveness of heat transfer processes. This work contributed towards new solar thermal system design for power generation in future.

(a)

(b)

(c)

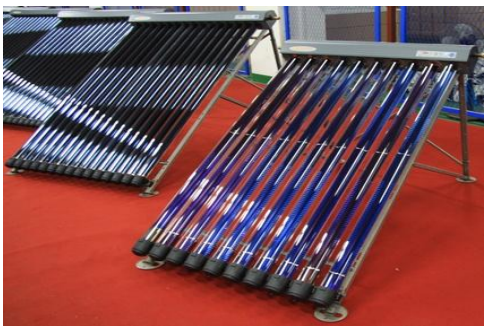

(d)

(e) **(f)**

Fig. 1.1 Present solar thermal technologies based on surface-absorption base receivers: a) linear parabolic trough b) linear Fresnel trough[2], c) Parabolic dish type[3], d) Evacuated tube collector[4], e) Solar pound[5], f) solar power tower[6].

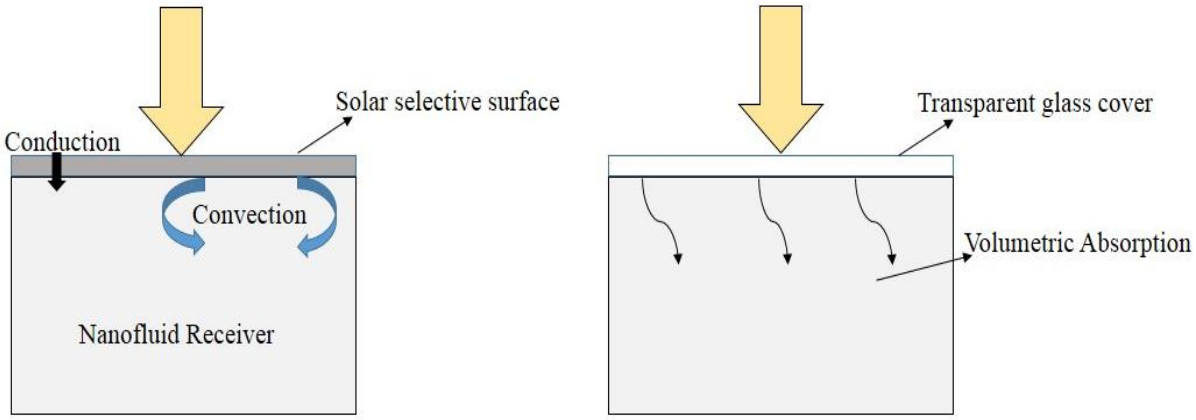

(a) **(b)**

Fig 1.2 Schematic of (a) surface based solar absorption receiver (b) volumetric based solar absorption receiver.

[1]http://www.energynext.in/indias-first-csp-plant-commissioned-under-jnnsm/

[2]https://csp-world.com/news/20131015/001222/first-year-operation-puerto-errado-2-fresnel-csp-plant

[3]https://www.pinterest.com/pin/490399846906567265/

[4]http://www.garagejournal.com/forum/showthread.php?t=78588

[5]https://solarthermalmagazine.com/learn-more/the-solar-pond/70-kwatts-in-elpaso-texas/

[6]https://www.pinterest.com/pin/372884044132238968

1.2 Literature survey

The generation of clean energy with minimal environmental impact is the key challenge facing society today. Energy development authorities predict that the world population needs 30 TW of energy supply by the year of 2050 to retain the economical escalation (SousaLd. Energy vision 2050, 2008). Sun irradiates adequate amount of energy on the earth surface per day, hourly solar flux incident on earth surface will be enough to achieve the energy demand for a year (Lewis, 2007).The literature review regarding nanofluid based volumetric solar receiver could be divided in two categories. The first category spotting the experimental and theoretical studies on the solar thermal system receiver using nanofluid as HTF and second study consist of numerical and experimental studies of optical and transport properties of nanofluid.

- **Modeling of volumetric solar receivers**

The investigation of linear parabolic solar collector performance by using nanofluid as the HTF is done (Khullar et al., 2010). The receiver modeled as 2-Dincompressible steady state system, and the finite difference technique was used to numerically solve the system of equation. They estimated all the governing parameters quantitatively and difference between the two cases (conventional parabolic collectors and nanofluid based collectors). That Study reveals that nanofluid based collector works efficiently than the conventional one collector under analogous working conditions. The performance of concentrated STS is estimated and compared with the conventional one (Taylor et al., 2011). They proved that the efficiency of collector enhanced by 10% might be possible by replacing the working fluid water with nanofluid. A low temperature nanofluid- based DASC theoretically investigated the influence of different parameter over efficiency (Tyagi et al., 2009). Their analysis tells that by dispersing nanoparticles with heat transfer fluid, the thermal efficiency enhanced significantly for small amount of volume fraction of nanoparticles. If volume fraction is greater than 2%, causes thermal efficiency remains unchanged, so by adding up more nanoparticles is not profitable. A numerical and experimentally analysis conducted on a micro scale DASC (Otanicar et al., 2010). They investigate the performance of a DASC for different nanofluids (carbon nanotube, graphite, and silver), after that they compared there result with conventional receiver, by adding small volume fraction (approximately 0.5%) remarkable improvement in the efficiency could be possible. An experimentally study confirm the consequence of Al_2O_3/water nanofluids on the efficiency of flat-plate solar

collector (Yousefi et al., 2012). They observe the effects of two different weight fractions of the nanofluid, with 0.2% and 0.4% and the diameter of particles was 15 nm. There was Improvement in efficiency around 28.3% for 0.2% volume fraction. Their results proved that the surfactant (Triton X-100) presence in the nanofluid extremely affects solar collector's efficiency, can be improved by 15.62%. Also it enhanced the stability of nanoparticles suspended in base fluid. An absolute study till now that combined experiment with the modeling of direct solar receiver (Lue et al., 2014). They prepared different kind of nanofluid (Texatherm oil as a base fluid) with sets of nanoparticles, and determined the optical properties of each fluid experimentally. The thermophysical properties of nanofluid (specific heat, thermal conductivity and viscosity) were determined by experiments and the optical were calculated using classical Mie Theory. This information incorporated in two dimensional model of small scale direct solar receiver and validated with the experimental results.

An analytical model of volumetric flow receiver with dispersed nanoparticles (graphite suspended in Therminol VP1) was proposed to investigate the effect of governing parameter on receiver efficiency and performance for solar thermal application (Veeraragavan et al., 2012). This study investigated suspended nanoparticles to absorb radiation and the effect of heat loss, particle loading, solar, Nusselt number, concentration and channel height on receiver efficiency. A different approach is conducted to solar energy harvesting by using nanofluids concentrated parabolic solar collector (Khullar et al., 2012). A theoretical model results confirmed that the nanofluid based receiver has the potential to harness the sun irradiation more efficiently than the conventional one. In addition, impact of nanoparticles size, shape and material over the thermal efficiency and maximum outlet fluid temperature. A similar study for concentrated solar flux and higher temperature solar thermal application is investigated (Lenert & Wang, 2012). A numerical model (one-dimensional) was developed to obtain the temperature variation along the model height and re-emission of energy from HTF at high temperature in case of direct nanofluid based solar collector. The model demonstrated that with the increase in nanofluid height and incident solar flux concentration the efficiency of the system increases extensively. When combined with power cycle, the optimal system efficiencies greater than 35% when C >100 and H >5cm.A three dimensional theoretical model was developed to identified the direct absorption of sun radiation in two different absorbing HTF like, gray (graphite nanoparticles in water) and non-gray(copper sulfate) fluids (Kaluri et al., 2015). Parametric studies were conducted on model and it was identified that by increasing the concentration ratio (CR) of the solar irradiation,

considerably increases the collector efficiency. It was found that for wall insulated collector, the efficiency enhanced by 12.9% and 28.8% with CR 48 and CR 683, respectively.

- **Properties of nanofluids**

Nano-scale metallic particles dispersed in conventional HTF known as 'Nanofluids', also a novel category of Nano-technology. Various literatures are available to understand the properties of nanofluids like transport properties, optical properties and stability of nanoparticles. The essential articles have been selected and their respective conclusion is included to explore the nanofluid importance in STS.

In recent study, researchers explore the performance of nanofluid in verity of applications and areas and future possibility to modify the present technology with nanofluid based system (Taylor, et al., 2013). Nanoparticles based fluid has improved absorption characteristics of sun light then the base fluid. Furthermore, thermal conductivity of conventional fluid drastically increases with the amount of nanoparticles suspended in base fluid in heat transfer application. Optical properties are depends on particle size, which influence the amount of absorbs solar radiation along with the thermal emission from the particles, small particle size increases the efficiency of the system (Otanicar et al., 2009). Also the optical properties of base fluid alter significantly with nanoparticles dispersion and their CR (Prasher & Phelan, 2005). Nanoparticles stability in the base fluid can be retain using plasma functionalized multi-walled carbon Nano-tubes (MWCNTs) in water, ethylene glycol, propylene glycol and Therminol VP-1 (Hordy et al., 2014). With MWCNTs, no agglomeration in nanoparticles is occur in case of water and glycol based nanofluids when heated at 85 and 170 ◦C, respectively, high level agglomeration can be occur non-polar Therminol VP-1 i.e. higher stability of nanofluid. Nanofluid optical properties were shows that by using MWCNTs in base fluid enhanced its absorbing characteristic, even at low concentration.

Table 1.1 Summary of results of solar thermal systems using nanoparticle dispersions.

Solar thermal system					
Concentrating type (CT)/Non concentrating type (NCT)	**Receiver Geometry**	**Nanopartcle Dispersion employed**	**Operating tempera-tures(°C)**	**Major findings** **E: Experimental** **M: Modeling**	**References**
CT, Potential application in central receivers	Cylinder D=0.0635 m, H=0.06m	C coated cobalt/ Therminol VP-1	**E**: 20-50**°C** **M**: 127-1127**°C**	**M**: 1. Receiver efficiency increases by increasing Nano-fluid optical thickness and incident Solar flux. 2. When coupled to a power cycle, combined optimal efficiencies exceeding 35% can be attained for $C_{ratio} > 100$ and $H > 5$ cm **E**: An experimental simulation matches with the numerical modeling results.	(Lenert and Wang, 2011)
NCT	Cuboid L=1.5 m W=1.5 m H=0.01 m	Hypothetical	**M**: 20-36**°C**	**M**: 1. Tailoring extinction profile as a function of depth improves thermal efficiency. 2. Efficiency improvement of 6% as compared to conventional surface absorption-based systems	Otanicar et al., 2011)
NCT	Cylinder D=0.035 m H=0.003 m	Gold nanoparticles (GNP)/Water	**E**: 20-34**°C**	**E:** 1. GNPs have good photo thermal conversion efficiency, at particle concentration of 0.15 ppm, GNP increases the photo thermal conversion efficiency of base-fluid by 20% and reaches a specific absorption rate of 10 kWg^{-1} 2. Photo thermal conversion efficiency increases with increasing volume fraction.	(Zhang et al., 2014)
NCT, Flat plate collector	Cuboid A=1.51 m^2	MWCNT/ Water	**E**: 30-40**°C**	**E:** Efficiency of solar collector increases as the pH is increased or decreased with respect to the Isoelectric point	(Yousefi et al., 2012a)
NCT, Flat plate collector	Cuboid A=1.51 m^2	Al2O3/Water	**E**: 30-40**°C**	**E**: Using 0.2 Wt% Al_2O_3 nanofluid as absorbing medium in a flat plate solar water heater increases the efficiency by28.3%	Yousefi et al., 2012b)
CT, Parabolic	Cuboid	Graphite/	E: 270°C	M: 1. In case of nanofluid based	(Taylor et

dish collector	L=0.02 m W=0.02 m H=0.001 m	Therminol VP- 1		receivers, efficiency enhancement of 10% can be achieved relative to surface absorption-based receivers when concentration ratios are in The range of 100-1000. 2. Graphite nanofluids with volume fraction on the order of 0.001% are suitable for 10- 100 MWe power plants. E: Experiments on laboratory scale nanofluid based dish receiver suggest that 10% increase in efficiency can be achieved relative to surface absorption collector if operating conditions are carefully chosen	al., 2011)
CT	Cuboid H=0.001m-0.01 m	Graphite/ Therminol VP- 1	----------	**M:** 1. An analytical model was formulated to investigate the effect of heat loss, particle loading and solar concentration and channel height on the receiver efficiency. 2. Model predicts an optimum total efficiency of 0.35 for a volumetric receiver (dimensionless receiver length of 0.86) employing graphite Nanoparticles dispersed.	(Veeraraga van van et al., 2012)
NCT	Cuboid H=0.001 m	Aluminium/ Water	**M:** 34-35°**C**	**M:** 1. Presence of nanoparticles Increases the absorption of incident radiation by more than nine times over that of pure water. 2. Under similar operating conditions, the efficiency of a direct absorption collector using nanofluid as the working fluid is found to be up to 10% higher that of conventional flat plate collector.	(Tyagi et al., 2009)
CT	Cuboid H=0.05cm	graphene/ionic liquid nanofluids	**E**=300-600K **M**=300-600K	**E:** An experimental model was used to quantify temperature profiles of 0.0005wt% and 0.001wt% of grapheme in BF4 for analogous fluid height7.5cm and3.8cm, the experimental results illustrates good agreement with the numerical outcome. **M:** The model confirms that there receiver thermal efficiency increases with solar concentration and receiver height.	(Liu, Ye, Zhang, Fang, & Zhang, 2015)

NCT	Cuboid H=10 mm	Silver nanofluids	**E:** 20 -50^{o} C **M:** 30 -52^{o} C	**E:** Efficiency of the collector increases with receiver height and NP concentration and then achieves a maximum value. However, the receiver efficiency drop as the irradiation time increases remaining to the improved heat loss. **M:** apart from various nanoparticles, model shows that gold and silver based nanofluids have higher efficiency then that of titanium dioxide nanofluid for same volume fraction. Furthermore, enhancement in the receiver efficiency can be achieved by engineering the absorption spectrum of the HTF to matches with the solar spectral intensity directly.	(Chen, He, Zhu, & Wen, 2016)
NCT	Cylinder	Cobalt oxide (Co3O4)	**E:** 20-70^{o} C	**E:** The work proposes that the application of Cobalt oxide (Co3O4) based nano-fluid absorption system for efficient conversion of radiative heat flux into useful thermal energy over that of surface absorption based system.	(Bhalla & Tyagi, 2017)

1.3 Aim and Objective of Thesis

The literature background shows that volumetric receiver promise to be more efficient than surface-based receiver, but prediction of this quantitative amount of increased efficiency can be complicated, even for relative simple geometries of volumetric receivers, numerous parameters play significant role. Present numerical model exist for volumetric solar receiver doesn't include radiative heat transfer accurately due to its complexity. In most of the models, scattering is generally neglected due to small particle size and analytical solution are used for the radiative heat transfer in the direction of the collimated radiation i.e. accurately parallel to rays of light. Also absorption and emission of the particle depends upon the direction and wavelength (i.e. non-gray surface), but models often use gray properties of surface. The analysis of flow model is required to capture the actual heat transfer rate through the receiver but till now plug flow is assumed or an analytical solution is available. In this thesis, all mentioned and novel physics of nanofluids are included in numerical model and solved by using finite difference method (FDM) in MATLAB. Furthermore, to quantify the absorption capability, solar weighted absorptivity of various nanoparticle dispersions have been computed by using DDSCAT Fortran-90 open package software.

The objective of this study is to contribute towards the development of volumetric flow receiver design with nanofluid inside the receiver and to quantify the effect of different parameter over the thermal efficiency of the receiver.

Chapter 2
Radiative and thermophysical properties of Nanofluid

2.1 Introduction

A Nanofluid is composed by the nanometer sized particles (generally 1 to 100 nm diameter size) suspended or dispersed in the base fluid. In the last two decades, the application of nanofluids has paying attention because of their reported better thermal performance and different potential applications. However, there are many contradictions reported experimentally, which conclusion shows that their thermophysical properties such as the effective thermal conductivity of nanofluids and disagreements in the underlying enhanced mechanisms. In this Chapter, various aspects of nanofluids such as synthesis, potential applications, experimental and analytical studies on the thermal conductivity, thermal diffusivity and convective heat transfer. In order to established the model of solar receiver in which nanofluid flow within the receiver, material properties are required.

2.2 Preparation and stability of Nanofluids

2.2.1 Preparation Method

The stability of nanofluids is the serious problem for designing a nanofluid based direct absorption system. The stability of nanoparticles dispersion basically depends upon the synthesis route of these nanofluids and also on operating conditions. In order to ensure the stability, it is required to know the methods of preparation of nanofluids. The method of preparation can be classified as a one-step process or a two-step process.

- One step process: the synthesis of nanofluid is formed when the nanoparticles and the base fluid made simultaneously. In this process, the problem of agglomerations minimized i.e. highly stable nanofluid synthesis formed.
- Two-step process: the synthesis of nanofluid is obtained by dispersing the already prepared nanoparticles with the base fluid. In first step, dry nanoparticles are produced to the desired size and shape by physical or chemical processes and secondly they mixed with base fluid by mechanical method such as vibration and ultra sonification.

2.2.2 Stability of nanofluids

Nanofluids can loss their heat transfer potential due to their tendency to agglomeration. Therefore, investigation of stability problem in mixture is an unavoidable issue that can significantly vary the thermophysical properties of nanofluids and also vital to examine the significant factors to the stability of these suspension. This section contains some stability advancement techniques and enhancement processes.

Stability evolution methods for nanofluids

- **Zeta potential analysis:** Zeta potential referred as the potential difference between the dispersion medium and the stationary layer of fluid attached to the particle, fundamentally it indicate the degree of repulsion between adjacent charged particles in dispersion. In general, nanofluids with zeta potential between 40-60 mV have excellent stability. Zeta potential technique (kim et al., 2009) is used to determine the stability of Au-water nanofluid and found out standing stability.
- **Sedimentation Method:** The method of sedimentation is the most elementary method for evaluation of nanofluids (Wei & Wang, 2010). In this method, an exterior field of force is generated to start the sedimentation of nanoparticles in the base-fluids, the volume or weight of sedimentation indicates the stability of nanofluids.
- **Spectral analysis method:** Spectral analysis is a further useful way to estimate stability of nanofluids via UV- spectrophotometer; UV-spectroscopy gives quantitative results matching to volume fraction of nanofluids. The analysis of stability of multi wall nanotube (MWNT) nanofluid done by quantifies the UV-vis absorption of MWNT for different sediment time (Hwang, et al., 2007).
- **Electron microscopy and light scattering methods:** Microscopy and light scattering techniques are two common methods for measuring the particle size distribution, also for observing particle aggregation. Very high resolution microscopy such as Transmission electron microscope (TEM) and scanning electron microscope (SEM) are applied to capture the digital image of nanoparticles, known as electron micrograph.

2.2.3 Stability enhancement procedures

- **Addition of surfactants:** surfactant molecules, generally applied to stabilize the nanofluids, surround the nanoparticles and form an envelope around the nanoparticles. By adding surfactants reduces the surface tension of host fluid and enhances the concentration of particles. The electromagnetic force of repulsion between there covered nanoparticles obstructs the possible agglomeration of nanoparticles hence improves the stability of nanoparticle dispersion. Problem of thermal degradation at high temperature reduces applicability in solar thermal application (Ghadimi et al., 2011).
- **Surface modification techniques:** This technique involves dispersion of functional nanoparticles in the fluid can provide long term stability of nanofluids. Plasma deposition process has been found to be very effective methods for surface modification of carbon nanotubes (CNTs), which impart controllable hydrophilicity to the CNTs and hence refining the stability of CNTs based dispersion. Recently researchers reported that nanoparticles dispersions employing plasma preserved multi-walled carbon nanotubes (MWCNTs) have excellent stability over extended periods of time (around 8 months) at very high temperature up to 170°C (Prasher & Phelan, 2005).
- **PH control of nanofluids:** The stability of nanoparticle dispersion is directly connected to its electro-kinetic properties; therefore, control over the pH of them can enhance stability due to strong repulsive forces. The pH value of nanofluid should be such that it is far away from the Isoelectric point (IEP), at IEP zeta potential of the fluid is zero. For stable dispersions the pH value should be such that the value of the zeta potential is adequately high (Khullar et al. 2017).

2.3 Radiative properties of nanofluids

The parametric study of Radiative properties of nanofluids is extremely important to what concerns solar thermal direct absorption systems. When the solar irradiation, such as electromagnetic waves, interacts with a participating medium, two distinct situations can be occur, simultaneously or not, absorption and scattering. These phenomena imparted the deviation in intensity of irradiation; also can change the direction of the radiation, depending upon the Radiative properties of the participating medium.

The decay of intensity is caused by the absorption and the scattering is caused either by reflection, refraction or diffraction of the irradiation due to presence of Nano-scale solid particles. To quantify the phenomena of intensity decay, an absorption coefficient can be considered, which is evaluated by an approximation by simply adding the absorption coefficient of the base fluid and its dispersed nanoparticles, as shown in Eq. 2.1.

$$k_{a\lambda,nf} = k_{a\lambda,bf} + k_{a\lambda,np} \tag{2.1}$$

The spectral extinction coefficient is the sum of spectral absorption coefficient and spectral scattering coefficient.

$$k_{e\lambda} = k_{a\lambda} + k_{s\lambda} \tag{2.2}$$

For base fluid, due to small size of molecules scattering can be neglected and the attenuation of intensity is only caused by absorption may be considered. In that case, the spectral absorption coefficient can be calculated by Eq.2.3.

$$k_{a\lambda} = \frac{4\pi\kappa}{\lambda} \tag{2.3}$$

Where κ denotes the index of absorption, the existence of small particles in fluids alter the nature of absorption, as well as scattering, hence some complex correlations are required. For very small particles diameter, the approximation of Rayleigh scattering can be applied (Bohren & Huffman, 2008). This approximation is valid when $\alpha << 1$ and $|m|\alpha << 1$, physically when the particle size is much smaller than the wavelength of radiation, where α is defined as the size parameter and given by Eq. 2.4.

$$\alpha = \frac{\pi D}{\lambda} \tag{2.4}$$

Where D is particle diameter and $m(n + i\kappa)$ is known as the normalized refractive index of the particles given by Eq.2.5,

$$m = \frac{m_{particle}}{n_{fluid}} \tag{2.5}$$

From equation the extinction coefficient is given by Eq. 2.6,

$$k_{e\lambda} = \frac{3 f_v Q_{e\lambda}(\alpha, m)}{D} \tag{2.6}$$

Here, f_v denotes the volume fraction of the particle, and $Q_{e\lambda}$ is the extinction efficiency. The extinction efficiency within the Rayleigh region is given by the subsequent relation (Bohren & Huffman, 2008).

$$Q_{e\lambda} = 4\alpha \ \mathrm{lm}\left\{\frac{m^2-1}{m^2+2}\left[1+\frac{\alpha^2}{15}\left(\frac{m^2-1}{m^2+2}\right)\frac{m^4+27m^2+38}{2m^2+3}\right]\right\}+\frac{8}{3}\alpha^4\left|\left(\frac{m^2-1}{m^2+2}\right)\right|^2 \quad (2.7)$$

Above expression of extinction efficiency contains two terms in right hand side. First term refer as absorption efficiency $Q_{a\lambda}$ and second known as scattering efficiency. By examining equation it is noted that the absorption efficiency of particle predominantly varies linear with particle size, this statement is true since particle size is very small i.e. $\alpha << 1$, also scattering efficiency changes with the fourth power of particle size. Now substitute the Eq. 2.4 and 2.7 in Eq.2.6 The following expression of for $k_{e\lambda}$ is obtained (Bohren & Huffman, 2008):

$$k_{e\lambda} = \frac{12\pi f_v}{\lambda} \ \mathrm{lm}\left\{\frac{m^2-1}{m^2+2}\left[1+\frac{\pi^2 D^2}{15\lambda^2}\left(\frac{m^2-1}{m^2+2}\right)\frac{m^4+27m^2+38}{2m^2+3}\right]\right\}+\frac{8\pi^4 D^3 f_v}{\lambda^4}\left|\left(\frac{m^2-1}{m^2+2}\right)\right|^2 \quad (2.8)$$

Finally, the net Radiative properties of nanofluid can be evaluated by using Eq.2.5 and 2.7. The overall extinction due to the nanofluid is the sum of individual contribution of nanoparticles and the base fluid.

2.4 Optical properties of glass

The optical properties of a matter determined the tendency how it will interact with light, light can be considered as form of electromagnetic waves and consisting of packets of energy called photon. The photon may delivered their energy to the materials (absorption), but photon of identical energy are immediately emitted by the material (reflection), photons may not interact with the material structure (transmission), also during transmission photons are changes in velocity (refraction).

The most common optical properties are:

- Bulk Properties: refractive index, optical dispersion
- Wavelength-dependent optical properties: colour
- Non-traditional, 'induced' optical effects: photosensitivity, phototropism, Faraday rotation.

In this analysis, clear glass properties are used in RTE, these glasses are partially transparent throughout the near ultraviolet, visible and near-infrared regions that compose the solar spectrum (0.3-3 μm). The reflectance and transmittance of these glasses very much more in the solar spectrum than in the far-infrared because of the FeO (ferrous oxide) in the raw materials or added to control and melting.

2.4.1 Reflection and Transmission from glass

Consider the plane wave propagating in nor-absorbing medium (air) with reflective index (n_1), which is incident on glass on a glass medium with reflective index ($n=n_2+ik_2$) as shown in Fig. 2.1, as the wave propagate and transmitted through the material, due to presence of medium polarization of the electrons and the speed of light is decreases and the beam of light diverted it incident direction.

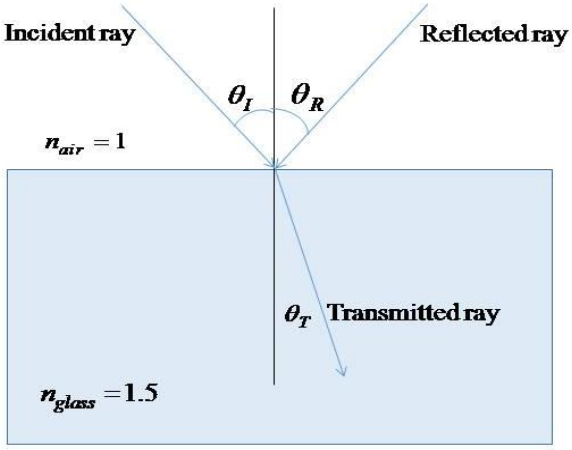

Fig. 2.1 Reflection and transmission of normally incident light

According to Snell's law of light refraction, reflective indices for light passing through from one medium (air) with reflective index n_{air} through a different reflective index n_{glass} is correlated to the incident and refractive angle by,

$$n_{air} \sin\theta_I = n_{glass} \sin\theta_R \tag{2.9}$$

For normal incidence, i.e. θ_I =0 the interface reflectance for normal incidence is listed as (Brewster, 1992)

$$R_g = \frac{(n_2 - n_1)^2 + k_2^2}{(n_2 + n_1)^2 + k_2^2} \tag{2.10}$$

In Eq. 2.10, reduced form of Fresnel relation, the value of n_1 depends upon the medium through which the normal intensity coming to the glass cover.

Table 2.1 Refractive indices of most common materials

Material	Refractive indices	Material	Refractive indices
Air	1.00	NaCl	1.54
Ice	1.309	Diamond	2.417
Water	1.33	Silicon	3.29
Silica glass	1.458	Germanium	4.00
Silicate glass	1.5	Therminol VP 1	1.667

The values of dielectric functions in this modeling for clear glass are taken from (Rubin, 1985) for far infrared and near visible region (0.3-30 μm). The normal transmittance of each glass cover can be written as,

$$T_g(d) = \frac{(1-R_n)^2 \exp(-k_{a\lambda} d)}{1-R_n^2 \exp(-2k_{a\lambda} d)} \tag{2.11}$$

Where d is the thickness of glass cover and $k_{a\lambda}$ is the absorption coefficient of glass cover. The spectral transmittance properties of glass cover depend on the thickness of glass cover and the spectral absorption properties of glass cover.

The fraction of beam intensity that is absorbed is connected with the thickness of the materials or fluid and the manner in which the waves interact with the material's structure. At any instance of wave passes through material, the overall intensity of the incident wave fall on the surface is equal to sum of the absorbed, reflected, and transmitted intensities over the surface. Finally the absorption coefficient can be calculated by Eq. 2.21 as follows,

$$A_g = 1 - T_g - R_g \tag{2.12}$$

2.5 Transport properties of nanofluids

The transport properties, also acknowledged as thermophysical properties, are properties which are used in the transport equation as well as in energy equation. The significant properties are the density, specific heat, viscosity and thermal conductivity.

- **Density (ρ):** The variation of density depends on the temperature and pressure, varies inversely with temperature. The density of a nanofluid can be calculated with

$$\rho_{nf} = (1 - f_v)\rho_f + f_v\rho_p \tag{2.8}$$

Here, ρ is the density and f_v is the volume fraction. The subscripts p, f and nf refer to the particle, fluid and nanofluid respectively.

- **Specific heat capacity (C_p):** The specific heat capacity of nanofluids should also consider the volumetric proportion of nanoparticles and base fluid, and it can be determined in the following way

$$C_{pnf} = \frac{f_v C_{pnp}\rho_{np} + (1 - f_v)C_{pbf}\rho_{bf}}{\rho_{nf}} \tag{2.9}$$

Table 2.2: Specific heat capacities of fluids and solids

Base fluid	C_p (KJ/Kg*K)	Solids	C_p (KJ/Kg*K)
Water	4.18	Alumina (Al_2O_3)	1.05
Ethylene glycol	2.42	Aluminum (Al)	0.90
Carbon tetrachloride	0.84	Copper	0.38
Glycerin	2.43	Gold	0.13
Therminol VP1	1.56	Silver	0.24
Perfecto HT 5	1.86	Graphite	0.71
Engine oil	1.19	MWCNT	0.75

- **Thermal conductivity (k):**

The thermal conductivity of a nanofluid may be calculated as an approximation using Eq. (2.10) which is valid not only for spherical but also for irregular particles, such as carbon

nanotube. This equation also takes into account the difference in the order of magnitude between the solid and the liquid thermal conductivities, given by the ratio $\frac{k_{np}}{k_{bf}}$,

$$k_{nf} = k_{bf}\left(1+\frac{f_v k_{np}}{3k_{bf}}\right) \tag{2.10}$$

- **Dynamic viscosity (μ):**

The dynamic viscosity is a transport property that can be determined for nanofluids using the following Eq. 2.11.

$$\mu_{nf} = \mu_{bf}\left(1+2.5\,f_v+6.5\,f_v^2\right) \tag{2.11}$$

Table 2.3: Values of thermophysical properties for different fluids and solids

Thermophysical properties	Fluid phase (water)	Cu (Copper)	Al_2O_3 (Alumina)	TiO_2 (Titanium)
C_p (J/KgK)	4179	385	765	686.2
ρ (Kg/m^3)	997.1	8933	3970	4250
k (W/mK)	0.613	400	40	8.9538
β (1/K)	21*10^-5	5.1*10^-5	2.4*10^-5	2.4*10^-5

Chapter 3

Mathematical Modeling of Volumetric Receiver

3.1 Introduction

In the present chapter, we shell developed the general relationship that governs the behavior of radiative heat transfer in the presence of an emitting and absorbing media by making a radiative energy balance, known as Equation of radiative Transfer (RTE), which describe the intensity of radiative flux within the enclosure as a function of location, direction and spectral variable. The modeling of combined thermal and radiative nature of solar receiver can be challenging because both these two equation are drastically different by nature. The RTE illustrated the ballistic transport of photon inside a medium which have defined optical thickness, whereas, heat transfer equation (HTE) describes the thermal diffusion of heat through molecular and lattice vibration. Here the coupled model of thermal and radiative phenomena is developed to predict the behavior of volumetric receivers at different operating condition. The model is used to predict temperature profiles inside the volumetric receiver, and estimate the amount of heat loss from the receiver, which quantified the efficiency of the receiver.

In this study, we have adopted fluid flow model between two finite plates for defining the thermophysical characteristic and heat transfer rate of nanoparticles based volumetric absorption concentrated solar thermal receiver, shown in Fig 3.1.

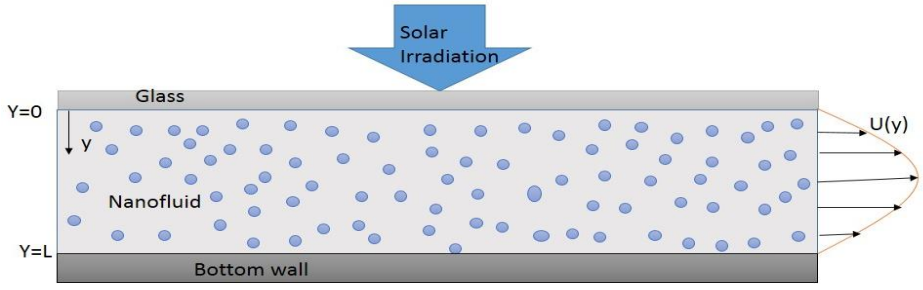

Fig 3.1 concentrating solar thermal receiver with suspended nanoparticles in HTF

The main purpose of this investigation was to present physical insight and to demonstrate and alternative approach to solve heat transfer problems by simultaneous conduction, convection and radiation. To do so a simple physical system was assumed, in which HTF passing through between two surfaces is separated by a variable height (H), top

surface covered with glass and bottom was insulated and opaque. The surfaces were assumed to be parallel to and extend indefinitely in normal and parallel direction to the plane of the figure. The glass and wall surface of the channel were assumed to specular reflector and diffuse emitters depends on their temperature. The heat transfer fluid (HTF) is enclosed at the top surface by the glass, which permits most of the irradiation of solar flux to pass through. This top surface is exposed to the ambient atmosphere and thus subjected to heat losses through convection.

The nanofluid was assumed to be an isotropic, homogeneous medium in local thermodynamic equilibrium, which absorbed and emit thermal radiation in a diffuse manner, and thermophysical properties assumed not to vary. The emissivity of both surfaces depends on respectively temperature. A general two-dimensional steady state heart transfer case is introduces and fully developed laminar flow considered reducing mathematical complication.

3.2 Analytical Solution of Radiative Transfer Equation

The Radiative intensity field falling on two dimensional flat plate collector because the temperature field present in the collector, and therefore associated with thermal emission. Thermal radiation is commonly used to describe the science of the heat transfer caused by electromagnetic waves. All phases (solid, gas and liquid) continuously emit and absorb electromagnetic waves, or photons, by lowering or raising their molecular energy levels. The strength and wavelengths of emission depend on the temperature of the emitting material. Solar thermal radiation approaches the earth surface is also the function of wavelength. Nanoparticles dispersed in HTF interact with the solar thermal radiation, these particle absorb and emit thermal radiation depending upon the spectral intensity. In case of volumetric solar absorbing receiver light travels throughout the medium with exponential decay of intensity along the optical depth.

In the recent theory, development of solar technology by using nanoparticles suspended in the HTF, it is necessary to develop a fundamental of radiation from nanoparticles at different wavelength (from electromagnetic theory).

3.2.1 Formal Solution of Equation of Radiative Transfer Equation in Plane-Parallel Geometry

Radiative transfer is basically classified as being either transfer between surface and transfer in participating media. Radiative transfer with in participating media is governed be the transfer equations. In nanoparticles dispersed media have the some influence of properties of particles like absorption, emission and scattering. Since, absorption and emission are

relatively simple to predict in mathematical form, compared to scattering. Form the basic law of electromagnetic theory it is proven that the intensity of the wave traveling to participating homogenous adsorbing medium is attenuated as the $\exp\left[K_{a\lambda} x\right]$. Where $K_{a\lambda}$ is the spectral absorption coefficient an x is the path length through wave travel, given as (Brewster, 1992)

$$K_{a_\lambda} = \frac{4\pi k}{\lambda_\circ} \tag{3.1}$$

The above exponential attenuation state that, when the emission not considered, along with Scattering, wave intensity I_λ obey the differential equation form

$$\frac{dI_\lambda}{dx} = -K_{a_\lambda} I_\lambda \tag{3.2}$$

Or for the general case,

$$I_\lambda(x) = I_O \exp\left[-\int_0^x K_{a_\lambda}(x')dx'\right] \tag{3.3}$$

Here $I_\lambda(x)$ is intensity at one direction, I_O is intensity at x=0. For absorbing, emitting, non-scattering medium, the transfer equation can be modified by considering the optical energy balance on the differential element along the single line of slight as shown in Fig 3.2.

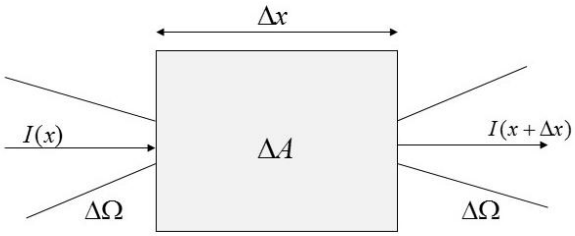

Fig 3.2 Energy balance on control volume along single line of sight

Applying energy balance on the element in the direction of Ω which gives,

Energy in + energy emitted = energy out + energy absorbed

In form of above notation,

$$I_\lambda(x)\Delta A\Delta\Omega + \varepsilon_\lambda(\Delta x) I_{b\lambda}(T)\Delta A\Delta\Omega = I_\lambda(x+\Delta x)\Delta A\Delta\Omega + \alpha_\lambda(\Delta x) I_\lambda(x)\Delta A\Delta\Omega \tag{3.4}$$

Now apply Kirchhoff law to simplify above equation, which states that emissivity is equal to absorptivity at constant temperature, and divided throughout by $\Delta A\Delta\Omega\,\Delta x$ in Eq.3.4. Hence reduced form of differential equation given as,

$$\frac{dI_\lambda}{dx} = -K_{a_\lambda} I_\lambda + K_{a_\lambda} I_{b\lambda} \tag{3.5}$$

Here Eq.3.5 represents the transfer equation of intensity for absorbing, emitting, non-scattering and homogenous medium. Since the major assumption was carried out while driving this equation is that the intensity is traveling in the single line of sight. But in actual cases the intensity sticks the medium at different solid angle and also the emission of medium always diffused in the medium (similar to black body). Hence to capture the essential physics of emission of nanoparticles it is assumed that they emitted radiation like back body. The spectral properties of incoming solar radiation and emitted radiation can be determined by the black body relation as given below,

$$I_{b\lambda}(T_{sun}, \lambda) = \frac{2hc_0^2}{\lambda\left[\exp\left(\frac{hc_0}{\lambda K_B T_{sun}}\right) - 1\right]} \tag{3.6}$$

Here, *h* denotes Planck's constant, K_B is the Boltzmann constant, c_0 is the speed of light in a vacuum and T_{sun} is taken as 5800 K.

3.2.2 Equation of radiative transfer for a plane-parallel slab

Consider the two parallel slabs, as shown in Fig 3.3, top surface of slab covered with glass envelope and insulated bottom surface having emissivity ε at constant temperatures. Now consider radiative heat transfer from a diffused glass surface across the non-scattering medium, the spacing between two surfaces is L. Solar irradiation is falling on the top of the glass surface and passes through nanofluid.

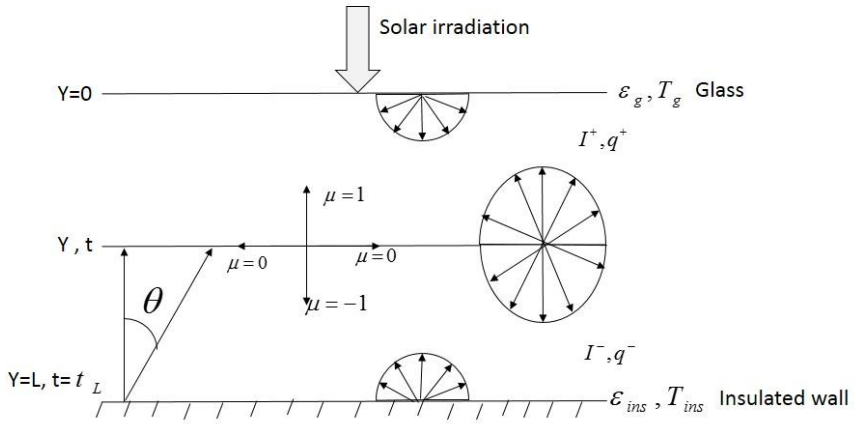

Fig 3.3 coordinates for formal solution of radiative balance in slab at any optical thickness

- **Optical Depth**

This is the important parameter used in radiative transfer in participating medium, also referred as opacity or turbidity. The optical depth is the integral of extinction coefficient along an optical line of sight.

$$t_\lambda = \int_0^y K_{e\lambda}(y')dy' \qquad (3.7a)$$

The optical depth is the non-dimensional path length for radiative transfer in a participating medium. For differential form it can be written as,

$$dt_\lambda = K_{e\lambda}dy \qquad (3.7b)$$

Optical depth is varying with angle of intensity travel. Form fig y= s μ and $\mu = \cos\theta$ .As the optical thickness increases, the mean free path of photons is reduced and approaches the black body limit. The optical thickness is the critical parameter in solving the RTE.

Similarly the intensity in the medium is a function of both optical thickness and direction.

$$I(t,\mu) = \begin{cases} I^+ \\ I^- \end{cases} \qquad (3.7c)$$

A + notation is used to specify the direction of intensity in the forward hemisphere (μ >0) and the – sign shows the intensity in the backward hemisphere (μ < 0).

- **Boundary conditions**

The boundary conditions at the glass cover is given by

$$I_\lambda^+(0,\mu) = S_\lambda(1-\rho_{g\lambda}-\alpha_{g\lambda}) + \rho_{g\lambda} I_\lambda^-(0,\mu) + \alpha_{g\lambda} I_{b\lambda}[T(0)] \quad (3.8a)$$

At the insulated surface intensity boundary condition become,

$$I_\lambda^-(H,\mu) = \rho_{w\lambda} I_\lambda^+(H,\mu) + \varepsilon_{w\lambda} I_{b\lambda}[T(H)] \quad (3.8b)$$

Here,

S_λ = Diffused Spectral incident radiation on the top layer of fluid,

$\rho_{g\lambda}$ $\alpha_{g\lambda}$ = Spectral Reflectivity and absorptivity of glass

$\varepsilon_{w\lambda}$ $\rho_{w\lambda}$ = Diffused Spectral Emissivity and reflectivity of insulated wall,

$I_{b\lambda}$ = Spectral Black body emission intensity

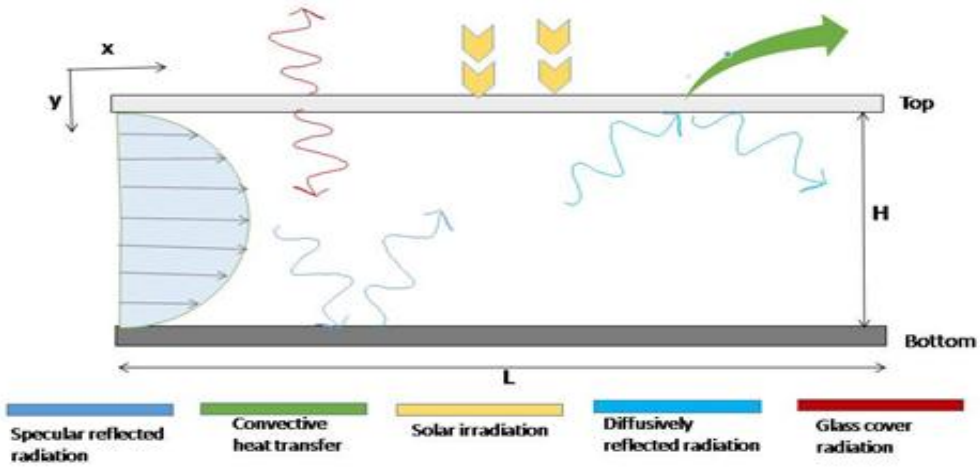

Fig. 3.4 Schamatic diagram of boundary condition for the receiver surfaces

In the Eq. 3.8a and 3.8b, there are four unknown intensity at the boundary of surface. Hence to solve these equations, we can use exponential attenuation of intensity.

$$I_\lambda^-(0,\mu) = I_\lambda^-(H,\mu)\exp\left[-\frac{t_H}{\mu}\right] \quad (3.9a)$$

$$I_\lambda^+(H,\mu) = I_\lambda^+(0,\mu)\exp\left[-\frac{t_H}{\mu}\right] \quad (3.9b)$$

Equation 3.9a represents the intensity at location top surface similarly 3.9b for bottom surface. After putting the value to equation 3.9 into 3.8, we get

$$I_\lambda^+(0,\mu) = S_\lambda\left[1-\rho_{g\lambda}-\alpha_{g\lambda}\right] + \rho_{g\lambda}\left(I_\lambda^-(H,\mu)\exp\left[-\frac{t_H}{\mu}\right]\right) + \alpha_{g\lambda} I_{b\lambda}[T(0)] \quad (3.10a)$$

$$I_\lambda^-(H,\mu)=\varepsilon_{w\lambda}I_{b\lambda}[T(H)]+\rho_{w\lambda}\left(I_\lambda^+(0,\mu)\exp\left[-\frac{t_H}{\mu}\right]\right) \quad (3.10b)$$

Now equation 3.10 can be simplified to get the directional intensity at both locations with the function of optical thickness.

$$I_\lambda^+(0,\mu)=\frac{S_\lambda\left[1-\rho_{g\lambda}-\alpha_{g\lambda}\right]+\rho_{g\lambda}\varepsilon_{w\lambda}I_{b\lambda}[T(H)]\exp\left[-\frac{t_H}{\mu}\right]+\alpha_{g\lambda}I_{b\lambda}[T(0)]}{1-\rho_{g\lambda}\rho_{w\lambda}\exp\left[-\frac{2t_H}{\mu}\right]} \quad (3.11a)$$

$$I_\lambda^-(H,\mu)=\varepsilon_{w\lambda}I_{b\lambda}[T(H)]+\frac{S_\lambda\rho_{w\lambda}\left[1-\rho_{g\lambda}-\alpha_{g\lambda}\right]\exp\left[-\frac{t_H}{\mu}\right]+\rho_{g\lambda}\varepsilon_{w\lambda}\rho_{w\lambda}I_{b\lambda}[T(H)]\exp\left[-\frac{2t_H}{\mu}\right]+\alpha_{g\lambda}\rho_{w\lambda}I_{b\lambda}[T(0)]\exp\left[-\frac{t_H}{\mu}\right]}{1-\rho_{g\lambda}\rho_{w\lambda}\exp\left[-\frac{2t_H}{\mu}\right]} \quad (3.11b)$$

Exact value to boundary intensity is given by Eq. 3.11; the source function and the properties of the boundaries in above equation is the function spectral wavelength.

- **Radiative heat flux at different optical thickness**

After computing the value of intensity at boundary, it is required to calculate heat flux at different optical thickness. First we calculate the intensity of radiative transfer at every location along the y co-ordinate system, as shown in Fig.3.5, the value to these intensity changes with the optical thickness of the slab. Now the transfer equation for slant path (s) become (Brewster, 1992)

$$\mu\frac{dI_\lambda(x,y,\mu,\phi)}{dt}=-I_\lambda(x,y,\mu,\phi)+I_{b\lambda}(T(x,y)) \quad (3.12)$$

Here μ is the cosine of the angle between the direction of the radiation intensity and the positive t axis. The boundary condition for Eq.3.12 can be written formally as now the solution of above equation obtained by using the integrating factor $\exp\left[-\frac{t}{\mu}\right]$ is

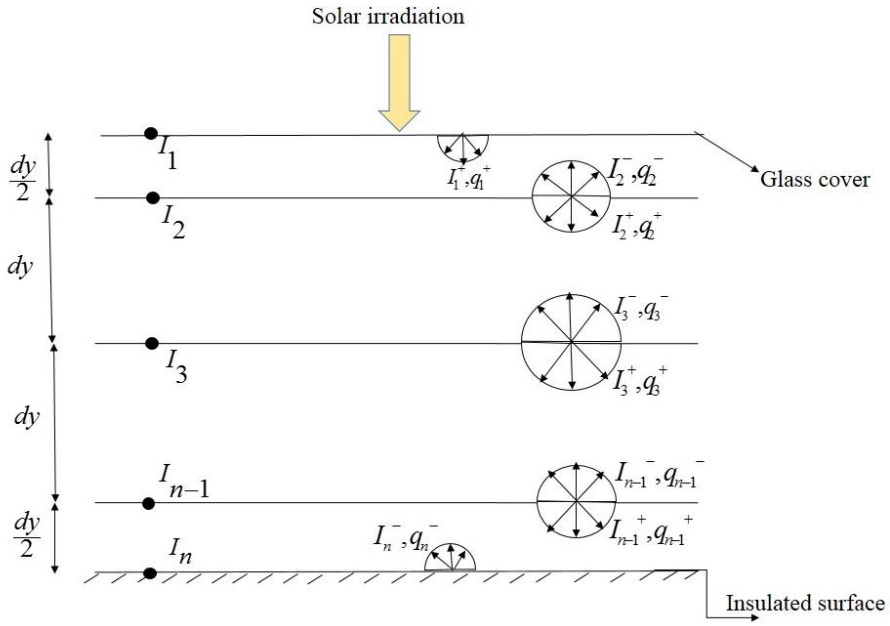

Fig. 3.5 Schematic of net radiative heat flux at different optical thickness

$$I_\lambda^+(t,\mu) = I_\lambda^+(0,\mu)\exp\left[-\frac{t}{\mu}\right] + \int_0^t I_{b\lambda}(t')\exp\left[-\left(\frac{t-t'}{\mu}\right)\right]\frac{dt'}{\mu} \qquad (3.13a)$$

$$I_\lambda^-(t,\mu) = I_\lambda^-(t_H,\mu)\exp\left[\left(\frac{t_H-t}{\mu}\right)\right] - \int_t^{t_H} I_{b\lambda}(t')\exp\left[-\left(\frac{t-t'}{\mu}\right)\right]\frac{dt'}{\mu} \qquad (3.13b)$$

For backward hemisphere ($\mu < 0$), put μ = - μ in Eq.3.13b we get,

$$I_\lambda^-(t,\mu) = I_\lambda^-(t_H,\mu)\exp\left[-\left(\frac{t_H-t}{\mu}\right)\right] + \int_t^{t_H} I_{b\lambda}(t')\exp\left[-\left(\frac{t'-t}{\mu}\right)\right]\frac{dt'}{\mu} \qquad (3.13c)$$

Above equation is integro-differential equation which solution is not straightforward. First term in the right hand side of the above Eq.3.13 correspond to the contribution to the intensity at location (t) in direction μ from the surface of glass and lower wall. The second terms on the right hand side of the Eq. 3.13shows the contribution of the intensity at location (t) in the direction of μ from the emission from the participating medium along the path between location t and the wall. Now the hemispherical fluxes at location t are determined by integrating the intensity field, using azimuthally symmetry. $d\Omega = 2\pi \times \mu d\mu$

$$q_\lambda^+(t,\mu) = 2\pi \int_0^1 I_\lambda^+ \mu d\mu \tag{3.14a}$$

$$q_\lambda^-(t,\mu) = 2\pi \int_0^{-1} I_\lambda^- \mu d\mu \tag{3.14b}$$

After Substituting Eq.3.13 into 3.14, we finally get spectral radiative heat flux

$$q_\lambda^+(t,\mu) = 2\pi \left[\int_0^1 I_\lambda^+(0,\mu) \exp\left[-\frac{t}{\mu} \right] + \int_0^1 \int_0^t I_{b\lambda}(t') \exp\left[-\left(\frac{t-t'}{\mu} \right) \right] \frac{dt'}{\mu} \right] \mu d\mu \tag{3.15a}$$

$$q_\lambda^-(t,\mu) = 2\pi \left[\int_0^{-1} I_\lambda^-(H,\mu) \exp\left[-\left(\frac{t_H - t}{\mu} \right) \right] + \int_0^{-1} \int_t^{t_H} I_{b\lambda}(t') \exp\left[-\left(\frac{t-t'}{\mu} \right) \right] \frac{dt'}{\mu} \right] \mu d\mu \tag{3.15b}$$

Equation 3.15 represents the forward and backward hemispherical flux at any optical depth in all direction. We can simplify further by putting Eq.3.11 in above Eq. 3.15. If we place spectral intensity at top location in forward hemispherical flux then we get

$$q_\lambda^+(t,\mu) = \pi \int_0^1 \left[\frac{S_\lambda \left[1-\rho_{g\lambda}-\alpha_{g\lambda} \right] \exp\left[-\frac{t}{\mu} \right] + \rho_{g\lambda}\varepsilon_{w\lambda} I_{b\lambda}\left[T(H) \right] \exp\left[-\frac{t_H + t}{\mu} \right] + \alpha_{g\lambda} I_{b\lambda}\left[T(0) \right] \exp\left[-\frac{t}{\mu} \right]}{1-\rho_{g\lambda}\rho_{w\lambda} \exp\left[-\frac{2t_H}{\mu} \right]} \right] \mu d\mu$$
$$+ 2\pi \left[\int_0^1 \int_0^t I_{b\lambda}(t') \exp\left[-\left(\frac{t-t'}{\mu} \right) \right] \frac{dt'}{\mu} \right] \mu d\mu \tag{3.16}$$

Integration of above equation is difficult to calculate; hence we can write dominator as $\left(1-\rho_{g\lambda}\rho_{w\lambda} \exp\left[-\frac{2t_H}{\mu} \right] \right)^{-1}$. We know the binomial theorem for negative integer is given by,

$$(x+1)^{-n} = 1 - nx + \frac{1}{2} n(n+1)x^2 - \frac{1}{6} n(n+1)(n+2)x^3 + \ldots\ldots\ldots\infty$$

Also we can write, $(x-1)^{-n} = 1 + nx + \text{ higher order term}$

After neglecting the higher order term dominator of Eq. 3.16 can be written by binomial theorem

$$\left[1-\rho_{g\lambda}\rho_{w\lambda} \exp\left[-\frac{2t_H}{\mu} \right] \right]^{-1} = 1 + \rho_{g\lambda}\rho_{w\lambda} \exp\left[-\frac{2t_H}{\mu} \right] \tag{3.17}$$

Hence we can replace the dominator of Eq.3.16 by Eq.3.17. Then we get,

$$q_\lambda^+(t,\mu)=\pi\int_0^1\left\{\begin{array}{l} S_\lambda\left[1-\rho_{g\lambda}-\alpha_{g\lambda}\right]\exp\left[-\frac{t}{\mu}\right]+\rho_{g\lambda}\varepsilon_{w\lambda}I_{b\lambda}\left[T(H)\right]\exp\left[-\frac{t_H+t}{\mu}\right]\times \\ +\alpha_{g\lambda}I_{b\lambda}\left[T(0)\right]\exp\left[-\frac{t}{\mu}\right]+S_\lambda\left[1-\rho_{g\lambda}-\alpha_{g\lambda}\right]\rho_{g\lambda}\rho_{w\lambda}\exp\left[-\frac{2t_H+t}{\mu}\right] \\ +\alpha_{g\lambda}\rho_{g\lambda}\rho_{w\lambda}I_{b\lambda}\left[T(0)\right]\exp\left[-\frac{2t_H+t}{\mu}\right]+\rho_{g\lambda}^2\rho_{w\lambda}\varepsilon_{w\lambda}I_{b\lambda}\left[T(H)\right]\exp\left[-\frac{3t_H+t}{\mu}\right] \end{array}\right\}\mu d\mu$$
$$+2\pi\left\{\int_0^1\int_0^t I_{b\lambda}(t')\exp\left[-\left(\frac{t-t'}{\mu}\right)\right]\frac{dt'}{\mu}\right\}\mu d\mu \qquad (3.18)$$

After solving the above equation positive hemispherical flux is calculated at optical depth (t) throughout the medium. The solution of Eq. 3.18 is complex to obtain straightforward, so it can be simplify ahead by using the exponential integral function.

The nth exponential integral function $\mathrm{E}_n(t)$ of the argument t is defined by

$$\mathrm{E}_n(t)=\int_0^1\mu^{n-2}\exp\left[-\frac{t}{\mu}\right]d\mu \qquad (3.19)$$

Here above Eq. 3.19 presents a useful relation for the functions $\mathrm{E}_n(t)$ with concise. This function has property that the derivative of Eq. 3.19 for n>2 gives (n-1) $^{\mathrm{Th}}$ order with negative exponential integral, and (n+1) th order in integration written as,

$$\frac{\partial\mathrm{E}_n(t)}{\partial t}=-\mathrm{E}_{n-1}(t) \qquad \int_t^\infty \mathbf{E}_n(t)dt=\mathbf{E}_{n+1}(t) \qquad (3.20)$$

Now replacing the Eq.3.18 with 3.19 results

$$q_\lambda^+(t,\mu)=\pi\left\{\begin{array}{l} 2S_\lambda\left[1-\rho_{g\lambda}-\alpha_{g\lambda}\right]\mathrm{E}_3(t)+\alpha_{g\lambda}I_{b\lambda}\left[T(0)\right]\mathrm{E}_3(t)+\rho_{g\lambda}\varepsilon_{w\lambda}I_{b\lambda}\left[T(H)\right]\mathrm{E}_3(t_H+t) \\ +2S_\lambda\left[1-\rho_{g\lambda}-\alpha_{g\lambda}\right]\rho_{g\lambda}\rho_{w\lambda}\mathrm{E}_3(2t_H+t)+\alpha_{g\lambda}\rho_{g\lambda}\rho_{w\lambda}I_{b\lambda}\left[T(0)\right]\mathrm{E}_3(2t_H+t) \\ +\rho_{g\lambda}^2\rho_{w\lambda}\varepsilon_{w\lambda}I_{b\lambda}\left[T(H)\right]\mathrm{E}_3(3t_H+t) \end{array}\right\}$$
$$+2\pi\left\{\int_0^t I_{b\lambda}(t')\,\mathrm{E}_2(t-t')dt'\right\} \qquad (3.21)$$

Equation 3.21 is the reduced form of radiative positive hemispherical flux at given optical thickness. Similarly the solution of negative hemispherical flux can be found by eliminating the negative intensity at bottom location in Eq. 3.15b by Eq. 3.11b in similar fashion as obtained Eq.3.21. Finally equation for negative flux at location (t) can be written as,

$$q_{\lambda}^{-}(t,\mu)=\pi\int_{0}^{-1}\left\{\begin{array}{l}\varepsilon_{w\lambda}I_{b\lambda}\left[T(H)\right]\exp\left[-\frac{t_H-t}{\mu}\right]+2S_{\lambda}\rho_{w\lambda}\left[1-\rho_{g\lambda}-\alpha_{g\lambda}\right]\exp\left[-\frac{2t_H-t}{\mu}\right]+\alpha_{g\lambda}\rho_{w\lambda}I_{b\lambda}\left[T(0)\right]\exp\left[-\frac{2t_H-t}{\mu}\right]\\+\rho_{g\lambda}\varepsilon_{w\lambda}\rho_{w\lambda}I_{b\lambda}\left[T(H)\right]\exp\left[-\frac{3t_H-t}{\mu}\right]+2S_{\lambda}\rho_{w\lambda}^{2}\rho_{g\lambda}\left[1-\rho_{g\lambda}-\alpha_{g\lambda}\right]\exp\left[-\frac{4t_H-t}{\mu}\right]+\rho_{w\lambda}^{2}\rho_{g\lambda}\alpha_{g\lambda}I_{b\lambda}\left[T(0)\right]\times\\\exp\left[-\frac{4t_H-t}{\mu}\right]+(\rho_{w\lambda}\rho_{g\lambda})^{2}\varepsilon_{w\lambda}I_{b\lambda}\left[T(H)\right]\exp\left[-\frac{5t_H-t}{\mu}\right]\end{array}\right\}$$

$$+2\pi\int_{0}^{-1}\int_{t}^{t_H}\left\{I_{b\lambda}(t')\exp\left[-\left(\frac{t-t'}{\mu}\right)\right]\frac{dt'}{\mu}\right\}\mu d\mu \qquad (3.22)$$

Equation 3.22 can be written in the form of exponential integral function.

$$q^{-}(t,\mu)=\pi\left\{\begin{array}{l}\varepsilon_{w\lambda}I_{b\lambda}\left[T(H)\right]\mathrm{E}_3(t_H-t)+2S_{\lambda}\rho_{w\lambda}\left[1-\rho_{g\lambda}-\alpha_{g\lambda}\right]\mathrm{E}_3(2t_H-t)+\alpha_{g\lambda}\rho_{w\lambda}I_{b\lambda}\left[T(0)\right]\times\\\mathrm{E}_3(2t_H-t)+\rho_{g\lambda}\varepsilon_{w\lambda}\rho_{w\lambda}I_{b\lambda}\left[T(H)\right]\mathrm{E}_3(3t_H-t)+2S_{\lambda}\rho_{w\lambda}^{2}\rho_{g\lambda}\left[1-\rho_{g\lambda}-\alpha_{g\lambda}\right]\mathrm{E}_3(4t_H-t)\\+\rho_{w\lambda}^{2}\rho_{g\lambda}\alpha_{g\lambda}I_{b\lambda}\left[T(0)\right]\mathrm{E}_3(4t_H-t)+(\rho_{w\lambda}\rho_{g\lambda})^{2}\varepsilon_{w\lambda}I_{b\lambda}\left[T(H)\right]\mathrm{E}_3(5t_H-t)\end{array}\right\}$$

$$+2\pi\int_{t}^{t_H}\left\{I_{b\lambda}(t')\mathrm{E}_2(t'-t)\right\}dt' \qquad (3.23)$$

The net spectral radiative heat flux at an optical depth can be determine by,

$$q_{net}^{\lambda}(t,\mu)=q_{\lambda}^{+}(0,\mu)-q_{\lambda}^{-}(0,\mu) \qquad (3.24)$$

After substituting the value of Eq. 3.21 and 3.23 in above Eq. 3.24, then the net heat flux at any optical depth can be written as

$$q_{net}^{\lambda}(t,\mu)=\pi\left\{\begin{array}{l}2S_{\lambda}\left[1-\rho_{g\lambda}-\alpha_{g\lambda}\right]\mathrm{E}_3(t)+\alpha_{g\lambda}I_{b\lambda}\left[T(0)\right]\mathrm{E}_3(t)+\rho_{g\lambda}\varepsilon_{w\lambda}I_{b\lambda}\left[T(H)\right]\mathrm{E}_3(t_H+t)\\+2S_{\lambda}\left[1-\rho_{g\lambda}-\alpha_{g\lambda}\right]\rho_{g\lambda}\rho_{w\lambda}\mathrm{E}_3(2t_H+t)+\alpha_{g\lambda}\rho_{g\lambda}\rho_{w\lambda}I_{b\lambda}\left[T(0)\right]\mathrm{E}_3(2t_H+t)\\+\rho_{g\lambda}^{2}\rho_{w\lambda}\varepsilon_{w\lambda}I_{b\lambda}\left[T(H)\right]\mathrm{E}_3(3t_H+t)\end{array}\right\}+2\pi\left\{\int_{0}^{t}I_{b\lambda}(t')\mathrm{E}_2(t-t')dt'\right\}$$

$$-\pi\left\{\begin{array}{l}\varepsilon_{w\lambda}I_{b\lambda}\left[T(H)\right]\mathrm{E}_3(t_H-t)+2S_{\lambda}\rho_{w\lambda}\left[1-\rho_{g\lambda}-\alpha_{g\lambda}\right]\mathrm{E}_3(2t_H-t)+\alpha_{g\lambda}\rho_{w\lambda}I_{b\lambda}\left[T(0)\right]\times\\\mathrm{E}_3(2t_H-t)+\rho_{g\lambda}\varepsilon_{w\lambda}\rho_{w\lambda}I_{b\lambda}\left[T(H)\right]\mathrm{E}_3(3t_H-t)+2S_{\lambda}\rho_{w\lambda}^{2}\rho_{g\lambda}\left[1-\rho_{g\lambda}-\alpha_{g\lambda}\right]\times\\\mathrm{E}_3(4t_H-t)+\rho_{w\lambda}^{2}\rho_{g\lambda}\alpha_{g\lambda}\times I_{b\lambda}\left[T(0)\right]\mathrm{E}_3(4t_H-t)+(\rho_{w\lambda}\rho_{g\lambda})^{2}\varepsilon_{w\lambda}I_{b\lambda}\left[T(H)\right]\mathrm{E}_3(5t_H-t)\end{array}\right\}-2\pi\int_{t}^{t_H}\left\{I_{b\lambda}(t')\mathrm{E}_2(t'-t)\right\}dt'$$

(3.25)

- **Radiative heat flux at top surface**

Since the receiver is enclosed by the surface trough which fluid is flowing with certain velocity and the solar irradiation is falling on the glass cover. Glass cover transmitted and emitted solar irradiation spectrally at different wavelength.

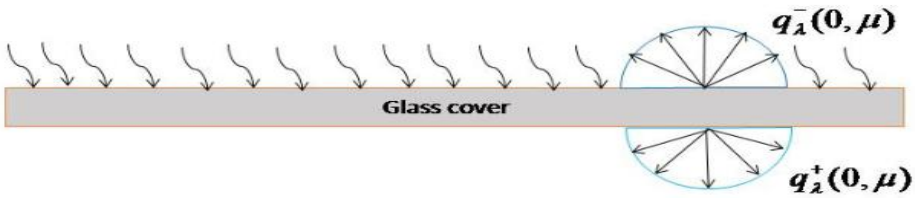

Fig 3.6 schematic of top glass covers boundary conditions

Hence to find net radiative heat flux can be determine by, as shown in fig.3.6

$$q_{net}^{\lambda}(0,\mu) = q_{\lambda}^{+}(0,\mu) - q_{\lambda}^{-}(0,\mu) \tag{3.26}$$

Where $q_{\lambda}^{+}(0,\mu)$ is the hemispherical flux, transmitted through glass and interact with participating medium and can be written as,

$$q_{\lambda}^{+}(0,\mu) = 2\pi\int_{0}^{1} \mathrm{I}_{\lambda}^{+}(0,\mu)\mu d\mu + 2\pi\int_{0}^{t_H} \rho_{g\lambda}\left\{I_{b\lambda}(t^{'})\mathrm{E}_2(t^{'}-t)\right\}dt^{'} \tag{3.27a}$$

The first term in Eq. (3.27a) capture the amount of flux at glass cover due to sun radiation, glass cover emission and intensity of bottom wall at glass cover, second term accounts the emission of fluid reflected back to medium.

Similarly flux at surface interact with atmosphere is the sum of bottom wall reflected intensity transmitted through glass and emission of glass itself. Hence can be written as,

$$q_{\lambda}^{-}(0,\mu) = 2\pi\int_{0}^{-1} \mathrm{I}_{\lambda}^{-}(0,\mu)\tau_{g\lambda}\mu d\mu + \pi\alpha_{g\lambda}\mathrm{I}_{b\lambda}\left[\mathrm{T}_g\right] + 2\pi\int_{0}^{t_H} \tau_{g\lambda}\left\{I_{b\lambda}(t^{'})\mathrm{E}_2(t^{'}-t)\right\}dt^{'} \tag{3.27b}$$

Now put Eq.3.27 into 3.26, which represents the positive and negative intensity at top location and finally the net radiative heat flux at glass cover, can be written in form of exponential integral function.

$$q_{net}^{\lambda}(0,\mu)=\pi\{S_{\lambda}[1-\rho_{g\lambda}-\alpha_{g\lambda}]+\alpha_{g\lambda}I_{b\lambda}[T(0)]+\rho_{g\lambda}\varepsilon_{w\lambda}I_{b\lambda}[T(H)]\mathrm{E}_3(t_H)+S_{\lambda}[1-\rho_{g\lambda}-\alpha_{g\lambda}]\rho_{g\lambda}\rho_{w\lambda}\mathrm{E}_3(2t_H)$$
$$+\alpha_{g\lambda}\rho_{g\lambda}\rho_{w\lambda}I_{b\lambda}[T(0)]\mathrm{E}_3(2t_H)+\rho_{g\lambda}^2\rho_{w\lambda}\varepsilon_{w\lambda}I_{b\lambda}[T(H)]\mathrm{E}_3(3t_H)\}+\int_0^{t_H}\rho_{g\lambda}\left\{I_{b\lambda}(t')\mathrm{E}_2(t'-t)\right\}dt'$$
$$-\pi\{\tau_{g\lambda}\varepsilon_{w\lambda}I_{b\lambda}[T(H)]\mathrm{E}_3(t_H)+S_{\lambda}[1-\rho_{g\lambda}-\alpha_{g\lambda}]\tau_{g\lambda}\rho_{w\lambda}\mathrm{E}_3(2t_H)+\tau_{g\lambda}\alpha_{g\lambda}\rho_{w\lambda}I_{b\lambda}[T(0)]\mathrm{E}_3(2t_H)$$
$$+\rho_{g\lambda}\rho_{w\lambda}\varepsilon_{w\lambda}\tau_{g\lambda}I_{b\lambda}[T(H)]\mathrm{E}_3(3t_H)+S_{\lambda}[1-\rho_{g\lambda}-\alpha_{g\lambda}]\tau_{g\lambda}\rho_{g\lambda}\rho_{w\lambda}^2\mathrm{E}_3(4t_H)+\alpha_{g\lambda}\rho_{g\lambda}\rho_{w\lambda}^2\tau_{g\lambda}I_{b\lambda}[T(0)]\mathrm{E}_3(4t_H)$$
$$+(\rho_{g\lambda}\rho_{w\lambda})^2\varepsilon_{w\lambda}\tau_{g\lambda}I_{b\lambda}[T(H)]\mathrm{E}_3(5t_H)+\int_0^{t_H}\tau_{g\lambda}\left\{I_{b\lambda}(t')\mathrm{E}_2(t'-t)\right\}dt'\}-\pi\alpha_{g\lambda}I_{b\lambda}[T(0)] \tag{3.28}$$

- **Radiative heat flux at bottom surface**

Figure 3.7 shows the bottom surface of the receiver which is optically and thermally insulated. Radiation intensity after passing through medium strikes the bottom wall and reflected back to the receiver which is again absorb by the participating medium.

Fig- 3.7 schematic of insulated wall bottom surface of the receiver

So that the net radiative heat flux at bottom wall become,

$$q_{net}^{\lambda}(H,\mu)=q_{\lambda}^{+}(H,\mu)-q_{\lambda}^{-}(H,\mu) \tag{3.29}$$

Here positive hemispherical flux become zero due to insulation, hence net flux is only due to emission and reflection of intensity by the wall,

$$q_{net}^{\lambda}(H,\mu)=-q_{\lambda}^{-}(H,\mu) \tag{3.30a}$$

$$q_{net}^{\lambda}(H,\mu)=-2\pi\int_0^{-1}\left[\mathrm{I}_{\lambda}^{-}(H)\right]\mu d\mu-2\pi\int_0^{t_H}\rho_{w\lambda}\left\{I_{b\lambda}(t')\mathrm{E}_2(t'-t)\right\}dt' \tag{3.30b}$$

After solving Eq. 3.30 for net radiative flux and replacing complex exponential term in form of exponential integral function. Finally the net radiative heat flux at bottom location can be written as,

$$q_{net}^{\lambda}(H,\mu)=-\pi\{\varepsilon_{w\lambda}I_{b\lambda}[T(H)]+2S_{\lambda}\rho_{w\lambda}[1-\rho_{g\lambda}-\alpha_{g\lambda}]\mathrm{E}_3(t_H)+\alpha_{g\lambda}\rho_{w\lambda}I_{b\lambda}[T(0)]\mathrm{E}_3(t_H)$$
$$+\rho_{g\lambda}\varepsilon_{w\lambda}\rho_{w\lambda}I_{b\lambda}[T(H)]\mathrm{E}_3(2t_H)+2S_{\lambda}\rho_{w\lambda}^2\rho_{g\lambda}[1-\rho_{g\lambda}-\alpha_{g\lambda}]\mathrm{E}_3(3t_H)$$
$$+\rho_{w\lambda}^2\rho_{g\lambda}\alpha_{g\lambda}I_{b\lambda}[T(0)]+(\rho_{w\lambda}\rho_{g\lambda})^2\varepsilon_{w\lambda}I_{b\lambda}[T(H)]\mathrm{E}_3(4t_H)+\int_0^{t_H}\rho_{w\lambda}\left\{I_{b\lambda}(t')\mathrm{E}_2(t'-t)\right\}dt' \tag{3.31}$$

3.2 Modeling of solar receiver

In order to find the temperature field and fluid flow inside the receiver tube when exposed to the solar irradiation the Navier-stokes (N-S) equations need to be solved. Due to presence of non-linearity in convective acceleration terms, it is difficult to handle N-S equations in physical situations. Since currently no general analytical schemes available to solve non-linear partial differential equations (PDEs). However, there are some modeling assumptions where the convective acceleration vanishes due to nature of interest or geometry of the flow system, hence the exact solution of such equation are often possible. The nature of N-S equation is applicable for both laminar and turbulent flows, the exact solution for laminar flows is obtained by considering the flow field independent of time (steady flow) and dependent on time (unsteady flow). Furthermore these categories solution of flow field can be applied to the type of flow like internal and external flows. In this chapter these governing (N-S and continuity) sets of equations will be solved for laminar, steady state, internal flow condition.

3.2.1 Modeling assumptions

The following general assumptions were made in order to reduce the general HTE and RTE that apply to volumetric receiver:

- Two- dimensional steady state laminar flow
- Fully developed laminar flow at the inlet of the receiver.
- Convective heat loss at the top side: For the convective heat loss to the surrounding atmosphere a constant ambient temperature T_{amb} is chosen with a constant convective heat transfer coefficient h_c.
- The horizontal direction of the receiver is assumed to be long as compared to height (H)
- Adiabatic bottom: no heat loss at the bottom of the receiver.
- The nanoparticles are assumed to be the same temperature as the HTF.
- The thermo-physical properties of the nanofluids are assumed to be the same as the bulk fluid.
- Natural convection inside the nanofluid due to temperature variation along the y-direction is neglected. However, natural convection may play a significant role in volumetric receiver when large temperature gradients are developed.

- The nanoparticles are assumed to stay suspended in the fluid for an indefinite period of time. They are assumed to flow with the HTF medium with negligible velocity slip.
- Only one interface between the ambient (n_1) and the nanofluids (n_2) is considered.
- Solar irradiation falling on the receiver normal to the top surface. Also the reflectivity of the top surface interface (y=0) is assumed to be zero for falling irradiation, but it reflect the emitted radiation from inside the receiver spectrally.
- The reflectivity of the bottom surface (y=H) is assumed to be spectrally specular, also act as diffuse emitter of absorbed radiation.
- The scattering from the nanoparticles is small compared to the absorbed radiation, which is consistent with the small size parameter ($\alpha << 1$) as discussed in chapter 2.
- Velocity variation along the x-direction is taken as constant.

3.2.2 Fully developed flow

The fully developed flow between two horizontal plates may be driven by gravity force or pressure force. If the channel held in horizontal position, gravity force has no effect except for hydrostatic pressure variation. The hydrostatic pressure difference between two locations of channel drive the flow while the viscous force gives the restraining force that properly balances the pressure force. The resulting phenomenon leads to the constant velocity (no acceleration) of fluid moving through channel. Fig shows the internal flow through the channel section. There is an entrance region length in which the upstream flow converges, the viscous boundary layer grows downstream merges from finite distance from inlet section and the inviscid core disappears, so making the flow completely viscous. The axial.velocity regulates till the entrance length is reached ($x=L_e$) and thus the velocity profile variation no longer changes in x-direction and only the function longitudinal direction, i.e. u=u(y). In this stage the flow is said to be fully developed flow in which the velocity and shear stress remains unchanged.

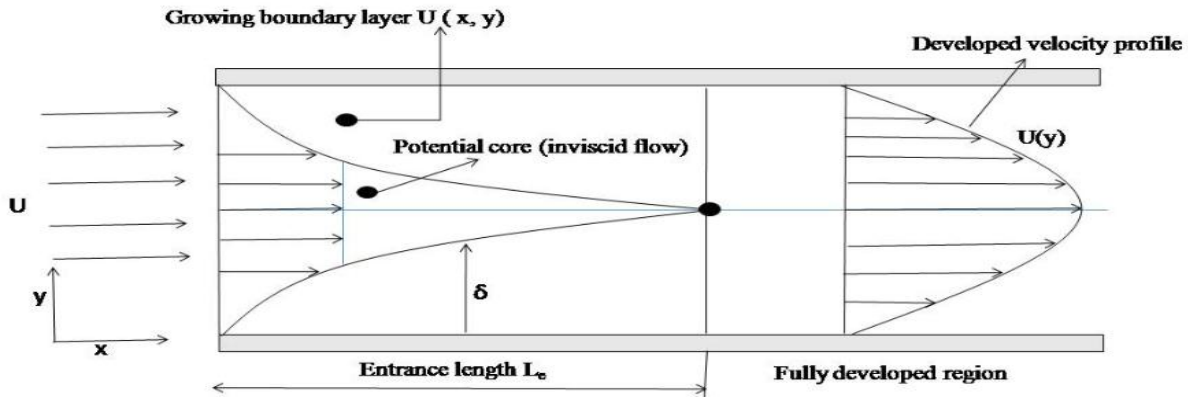

Fig 3.8 schematic of entrance length and velocity profile for fully developed flow

- **Viscous Incompressible laminar flow with Pressure Gradient between two parallel plates**

Consider the two-dimensional, incompressible flow; laminar viscous flow between two parallel plates with height (H) as shown in Fig.3.9, here the both plates are fixed and the pressure is varies along the x-direction. It is assumed that the plate is closely separated and sufficient long so that flow is essentially axial ($u \neq 0, v = 0, w = 0$). Furthermore, the flow is considered far away downstream from the inlet section so it can be treated as fully developed flow.

The continuity equation is written as,

$$\frac{\partial u}{\partial x} + \frac{\partial v}{\partial y} + \frac{\partial w}{\partial z} = 0; \rightarrow \frac{\partial u}{\partial x} = 0; \rightarrow u = u(y) \text{ only} \tag{3.32}$$

As it is obvious from Eq.3.32, that there is only one non-zero velocity components that is varies along the channel height. Now momentum equation for this planer flow section in x and y direction can be written as,

$$\rho\left(u\frac{\partial u}{\partial x} + v\frac{\partial u}{\partial y} + w\frac{\partial u}{\partial z}\right) = \rho g_x - \frac{\partial p}{\partial x} + \mu\left(\frac{\partial^2 u}{\partial x^2} + \frac{\partial^2 u}{\partial y^2} + \frac{\partial^2 u}{\partial z^2}\right) \tag{3.33a}$$

$$\rho\left(u\frac{\partial v}{\partial x} + v\frac{\partial v}{\partial y} + w\frac{\partial v}{\partial z}\right) = \rho g_y - \frac{\partial p}{\partial y} + \mu\left(\frac{\partial^2 v}{\partial x^2} + \frac{\partial^2 v}{\partial y^2} + \frac{\partial^2 v}{\partial z^2}\right) \tag{3.33b}$$

The momentum equation for respective direction reduces as follows,

X-momentum: $$\mu\frac{d^2u}{dy^2}=\frac{\partial p}{\partial x}=\frac{dp}{dx}$$

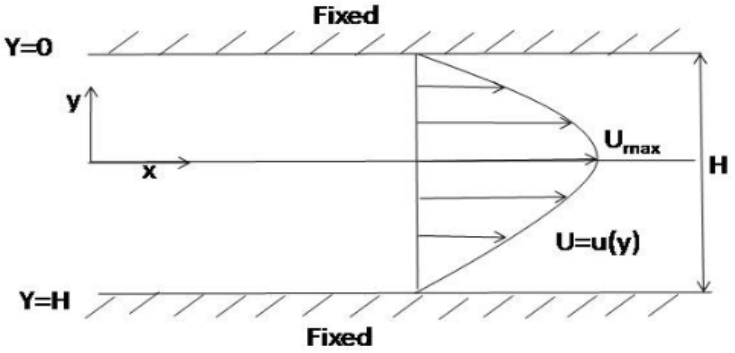

Fig-3.9 Incompressible viscous flow between two plates with pressure gradient

From x-momentum equation, it could be notable that the left hand side term contains variation of u with along the y- direction while the right hand side denoted the variation of pressure (p) with x. it must lead to same constant otherwise they will depends on each other. Since the flow has to overcome with wall shear stress and hence pressure must decreases in the flow direction, the constant must be negative quantity. Now the final form equation obtained for a pressure gradient flow between two parallel plates is written as,

$$\mu\frac{d^2u}{dy^2}=\frac{dp}{dx}=\text{constant}<0 \qquad (3.34)$$

The solution of Eq.3.34 can be obtained by double integration;

$$u=\frac{1}{\mu}\left(\frac{dp}{dx}\right)\left(\frac{y^2}{2}\right)+C_1y+C_2 \qquad (3.35)$$

The constant in equation can be found by applying the no-slip boundary condition at each wall,

at y=0, u=0; at y=H, u=0;

$$C_2=0 \text{ or } C_1=-\frac{1}{\mu}\left(\frac{dp}{dx}\right)\left(\frac{H}{2}\right)$$

After substituting these constant in equation, the general solution of Eq.3.35 can be obtained,

$$u(y)=\frac{1}{\mu}\left(\frac{dp}{dx}\right)\left[1-\frac{H}{y}\right]y^2 \qquad (3.36)$$

The mass flow rate ($\dot{m}$) passing between plates is calculated from the relationship as follows;

$$\dot{m} = \int_0^H \rho u dy = \int_0^H \rho \frac{1}{\mu}\left(\frac{dp}{dx}\right)\left[1-\frac{H}{y}\right] y^2 dy \tag{3.37}$$

If the Δp represents the pressure-drop between two points at a distance L along x-direction, then the Eq.3.37 is expressed as,

$$\dot{m} = \int_0^H \rho u dy = \int_0^H \rho \frac{1}{\mu}\left(\frac{\Delta p}{L}\right)\left[1-\frac{H}{y}\right] y^2 dy \tag{3.38}$$

Pressure loss Δp along the length of channel can be determined by the Darcy–Weisbach equation, which can be written as Eq.3.39,

$$\Delta p = \Gamma\left(\frac{\rho v^2}{2}\right)\left(\frac{L}{D_H}\right) \tag{3.39}$$

In Eq.3.39, Γ represents the fraction factor which depends on surface roughness and flow velocity, D_H hydraulic diameter of channel.

3.2.3 Generalized energy balance equation

The energy balance caused by the transportation of mass due to flow of the fluid within the solar thermal collector is incorporated by the definition that the collector's temperature depends on the coordinate in the direction of the fluid flow. The governing equations were derived by applying the energy balance for each discretized domain in the analyzed control volume of the solar collector.

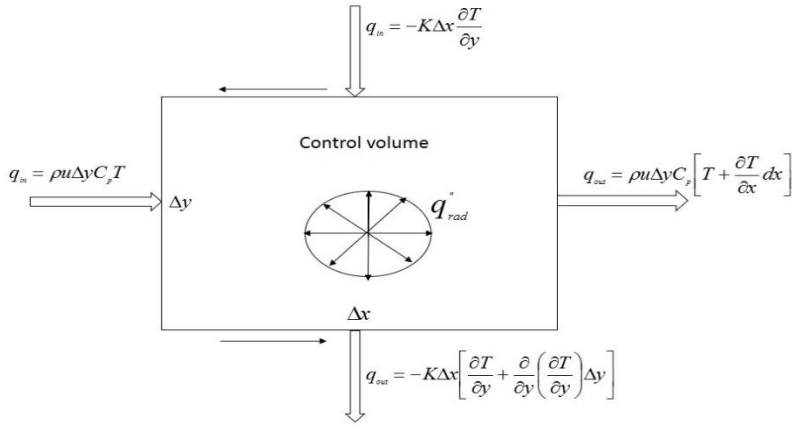

Fig 3.10 Energy balance on control volume with radiative losses

For two-dimensional heat transfer, the general energy balance is given by:

$$\dot{E}_{in} - \dot{E}_{out} + \dot{E}_{gen} = \dot{E}_{Stored} \tag{3.40}$$

After applying the principal of conservation of energy over the control volume, and substitute these values to general energy balance Eq. 3.40, we get

$$m(y)C_p \frac{\partial T}{\partial x} + K\frac{\partial^2 T}{\partial y^2} + \mu\left(\frac{\partial u}{\partial y}\right)^2 = \left(\frac{\partial q''_{rad}}{\partial y}\right) \tag{3.41}$$

The Eq. 3.41 represents the contribution of each individual energy transport phenomena, it is assumed that the x-direction conductive and radiative heat fluxes are negligible and the physical properties are constant. The term on the Left-hand side of the Eq.3.41 illustrates the heat transfer due to advection (convection) of thermal energy (plus flow work), conduction and viscous dissipation effects. The dissipation function Φ is associated with energy dissipation due to friction. It is important in high speed flow and for very viscous fluids. In Cartesian coordinates Φ is given by

$$\Phi = 2\left[\left(\frac{\partial u}{\partial x}\right)^2 + \left(\frac{\partial v}{\partial y}\right)^2 + \left(\frac{\partial w}{\partial z}\right)^2\right] + \left[\left(\frac{\partial u}{\partial y} + \frac{\partial v}{\partial x}\right)^2 + \left(\frac{\partial v}{\partial z} + \frac{\partial w}{\partial y}\right)^2 + \left(\frac{\partial w}{\partial x} + \frac{\partial u}{\partial z}\right)^2\right] - \frac{2}{3}\left(\frac{\partial u}{\partial x} + \frac{\partial v}{\partial y} + \frac{\partial w}{\partial z}\right)^2 \tag{3.42}$$

For highly viscous fluid the viscosity of the fluid will take energy from the motion of the fluid i.e. kinetic energy and converted into internal thermal energy of the fluid, it means gaining the energy of the fluid. This process is moderately irreversible and is referred to as dissipation, or viscous dissipation. The term of the right hand side of Eq.3.41, known as divergence of radiative heat flux, which gives the rate of net radiative flux leaving the control volume.

3.3 Numerical Algorithm

3.3.1 Radiative Transfer Equation

The equation of transfer, Eq.3.12, along with its corresponding boundary conditions, Eq.3.11, is solved by using the two-flux model. In this approach it's assumed that the intensity is constant over the various subinterval of the range $-1 \le \mu \le 1$. In the two-flux model, also known as the Schuster-Schwarzschild approximation (Chandrasekhar 1960), the intensity distribution is assumed to be semi-isotropic as shown in Fig. 3.11. The two-flux method is based on a simple physical model in which the positive-direction and negative-direction

radiative intensity are each assumed isotropic over their respective hemisphere of solid angles. Anisotropic scattering can be considered, but is used as an integrated average fraction for forward and backscattering. The method works well in one-dimensional systems, where it is simple to apply.

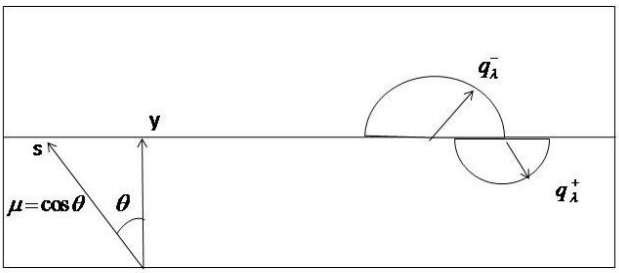

Fig. 3.11 Schematic of two flux model

3.3.2 Energy Equation

The finite difference method is used to solve energy equation, Eq.3.41, which is a second order differential equation, the divergence of radiative heat flux is treated as a volumetric heating source and can be easily determine by RTE. This method consists on the approach of the continuous conduction and convection heat transfer area on a set of discrete points, given by the intersection of horizontal and vertical lines. However, once there is also heat transfer on x direction, a two-dimensional mesh on x and y direction can be created, as shown in Fig. 3.12, in which n represents the position of the horizontal planes on y direction and m denotes the position of vertical plane in x direction, and these planes were assumed equidistant and parallel to the receiver's borders.

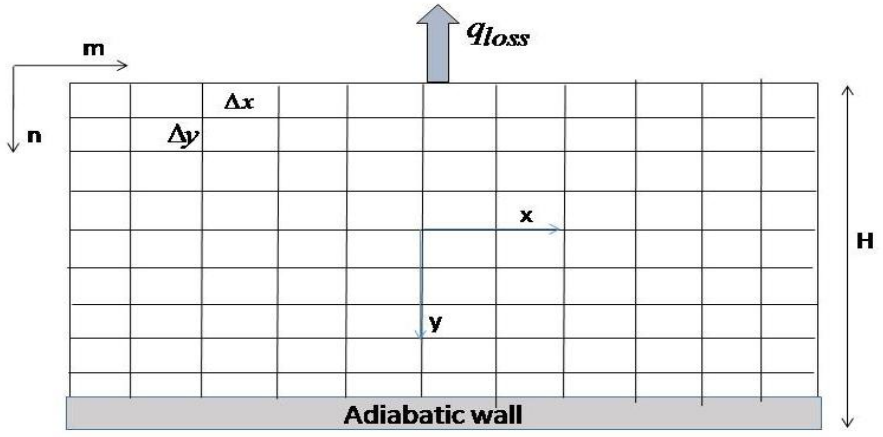

Fig. 3.12 Two-Dimensional mesh on the volumetric receiver

As a result of the spatial discretization, the temperature distribution is now represented by a finite number of temperatures. However, to determine the temperature in steady state outlet condition, space domain also needs to be discretized. The simplest way is to divide space in x direction into a set of constant intervals (Δx). The implicit method approximates the spatial derivative of temperature from Eq. 3.41 on a finite difference, by comparing the temperature at the moment m and the temperature on the consecutive instant, represented by m+1:

$$\frac{\partial T}{\partial x} = \frac{T_{m+1}^{n} - T_{m}^{n}}{\Delta x} \tag{3.43}$$

The advantage of using implicit scheme discretization is that, they are inherently stable (i.e. unconditional stable solution) for all combination of Δx and Δy, hence it eliminate the complexity involve in stability of numerical solution.

Finally, the temperature profile of the receiver in spatial regime can be determined by solving the energy balances on each horizontal and vertical plane ($\Delta x \times \Delta y$) and on each spatial space. Note that each temperature does not represent the temperature over a particular horizontal plane but the temperature associated to a small region around the plane. Top and bottom node considered as half node and interior node taken as full node, also the incident solar irradiation intensity node and temperature node are located in different location, as shown in Fig. 3.13.

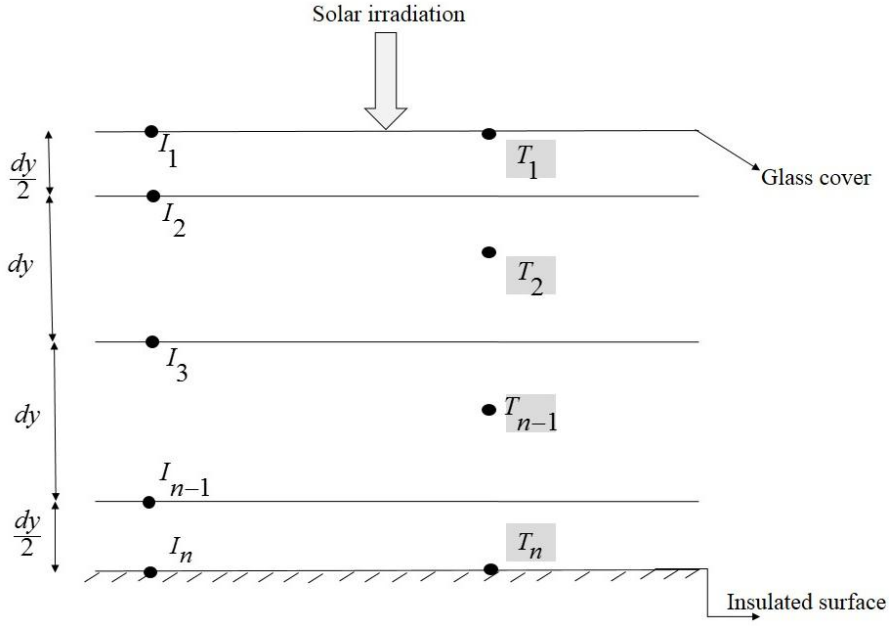

Fig. 3.13 schematic diagram of intensity and temperature node

Considering the stipulation where index n increases in the top to bottom direction and index m increases from inlet to outlet of the receiver, and that the flux on energy balance is positive when pointing towards the horizontal plane, three different situations can occur according to the geometry of Fig. 3.12: surface with convection (top), adiabatic surface (bottom), and internal plane.

- **Glass cover boundary surface (y=0)**

The convective losses take place from the top surface to the glass exposed to the atmosphere; these losses are the function of atmospheric temperature and other conditions. Now applying the heat energy balance to the top surface zone, see Figure 3.14, results the following equation:

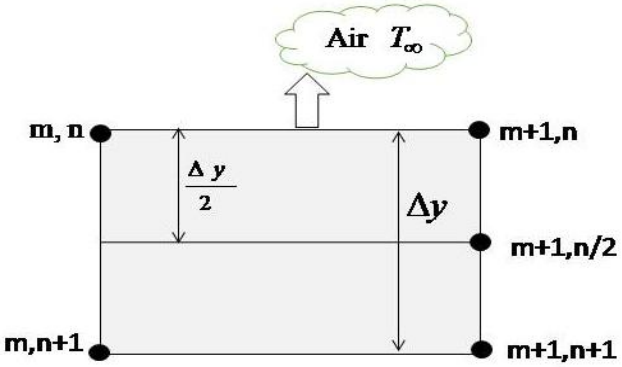

Fig. 3.14 Two- dimensional mesh grid points at top surface for volumetric receiver

$$h\Delta x\left(T_{m+1}^{n}-T_{\infty}\right)+m(y)c_{pnf}\left(\frac{T_{m+1}^{n}-T_{m}^{n}}{\Delta x}\right)=k_{nf}\left(\frac{T_{m+1}^{n+1}-T_{m+1}^{n}}{\Delta y}\right)-\frac{\partial q_{m+1}^{n}}{\partial y}+\mu_{nf}\left(\frac{u_{m+1}^{n/2}-u_{m+1}^{n}}{\Delta y/2}\right)^{2} \quad (3.44)$$

The Eq. 3.44 listed the overall energy balance at the top surface of the receiver. Where h is the convective plus radiative heat transfer coefficient, k is the thermal conductivity of nanofluid c_p is the specific heat of nanofluids and μ denotes the dynamic viscosity of nanofluid. The convection heat transfer coefficient depends on the air speed and receiver length (L) on x direction, while the radiation heat transfer coefficient is temperature dependent

Solving energy balance equation in order to the temperature at the instant m+1, we obtain

$$T_{m+1}^{n}\left(h\Delta x+\frac{m(y)c_{pnf}}{\Delta x}+\frac{k_{nf}}{\Delta y}\right)=T_{m+1}^{n+1}\left(\frac{k_{nf}}{\Delta y}\right)+T_{m}^{n}\left(\frac{m(y)c_{pnf}}{\Delta x}\right)+T_{\infty}\left(h\Delta x\right)-\frac{\partial q_{m+1}^{n}}{\partial y}+\mu_{nf}\left(\frac{u_{m+1}^{n/2}-u_{m+1}^{n}}{\Delta y/2}\right)^{2} \quad (3.45)$$

- **Adiabatic wall surface (y=H)**

The bottom wall of the receiver is optically and thermally insulated, also there is no convective losses from the insulated wall. It is assumed that the wall act as a specular reflector and diffused emitter. Applying the heat energy balance to the bottom surface zone, as shown in Fig. 3.15, results the following equation:

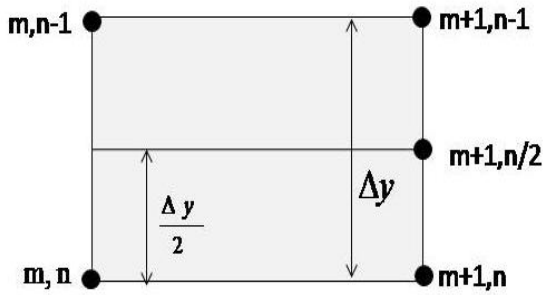

Fig. 3.15 Two- dimensional mesh grid points at bottom surface for volumetric receiver

$$m(y)c_{pnf}\left(\frac{T_{m+1}^{n}-T_{m}^{n}}{\Delta x}\right)=k_{nf}\left(\frac{T_{m+1}^{n-1}-T_{m+1}^{n}}{\Delta y}\right)-\frac{\partial q_{m+1}^{n}}{\partial y}+\mu_{nf}\left(\frac{u_{m+1}^{n/2}-u_{m+1}^{n}}{\Delta y/2}\right)^{2} \tag{3.46}$$

The Eq. 3.46 listed the overall energy balance at the bottom surface of the receiver. Where k is the thermal conductivity of nanofluid, mass flow rate is the function of location along y-direction which further depends upon the velocity profile of nanofluids and μ denotes the dynamic viscosity of nanofluid.

Solving energy balance equation in order to the temperature at the instant m+1, we obtain

$$T_{m+1}^{n}\left(\frac{m(y)c_{pnf}}{\Delta x}+\frac{k_{nf}}{\Delta y}\right)=T_{m+1}^{n+1}\left(\frac{k_{nf}}{\Delta y}\right)+T_{m}^{n}\left(\frac{m(y)c_{pnf}}{\Delta x}\right)-\frac{\partial q_{m+1}^{n}}{\partial y}+\mu_{nf}\left(\frac{u_{m+1}^{n/2}-u_{m+1}^{n}}{\Delta y/2}\right)^{2} \tag{3.47}$$

- **Internal plane**

The discretized node points in internal plane, as shown in fig. 3.16, are used to find the temperature field inside the receiver. The interior nodes are separated by Δy distance and equally distributed regions. The Eq. 3.48 represents the overall energy conservation in internal plane,

$$m(y)c_{pnf}\left(\frac{T_{m+1}^{n}-T_{m}^{n}}{\Delta x}\right)=k_{nf}\left(\frac{T_{m+1}^{n+1}-T_{m+1}^{n}}{\Delta y}\right)+k_{nf}\left(\frac{T_{m+1}^{n-1}-T_{m+1}^{n}}{\Delta y}\right)-\frac{\partial q_{m+1}^{n}}{\partial y}+\mu_{nf}\left(\frac{u_{m+1}^{n+1}-u_{m+1}^{n-1}}{\Delta y/2}\right)^{2}$$

(3.48)

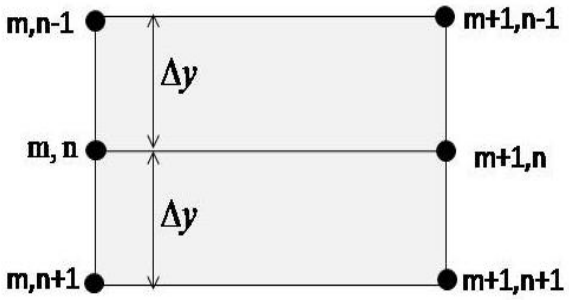

Fig. 3.16 Two- dimensional mesh grid points at internal surface for volumetric receiver

Again solving energy balance equation in order to the temperature at the instant m+1, we obtain

$$T_{m+1}^{n}\left(\frac{m(y)c_{p_{nf}}}{\Delta x}+\frac{2k_{nf}}{\Delta y}\right)=T_{m+1}^{n+1}\left(\frac{k_{nf}}{\Delta y}\right)+T_{m+1}^{n-1}\left(\frac{k_{nf}}{\Delta y}\right)+T_{m}^{n}\left(\frac{m(y)c_{pnf}}{\Delta x}\right)-\frac{\partial q_{m+1}^{n}}{\partial y}+\mu_{nf}\left(\frac{u_{m+1}^{n+1}-u_{m+1}^{n-1}}{\Delta y/2}\right)^{2}$$

(3.49)

3.4 Solution procedure

The governing equations of convective heat transfer and thermal radiation heat transfer in the direct absorption receiver are solved in the Cartesian coordinate system. The divergence of radiative heat flux is obtained by two- flux model, the net radiative heat flux at the internal plane is at different location can be calculated by using Eq. 3.25 and the radiative flux at the boundaries is obtained from Eq. 3.28 and 3.31. The Eq. 3.45, 3.47 and 3.49 can be used to compute the temperature field by marching forward in the x-direction. Since the radiative heat flux and its divergence at location x_{m+1} are not acknowledged before the temperature at this x-location is computed, hence energy equations cannot be used directly. Now the approximate forms of the energy equations are then used which are obtained by replacing the value of the radiative flux and its divergence at x_{m+1} by the values obtained at the previous node x_m. The above discretized energy equation forms a tri-diagonal linear algebraic system of equations which can be solve by using the matrix method, and its approximate forms can be used together in an iterative scheme. Fig. 3.17 shows the algorithm of code execution to

solve the problem, In order to save computation time, the momentum equation is resolved first and then energy equation and RTE are solved. The energy equation and RTE are coupled

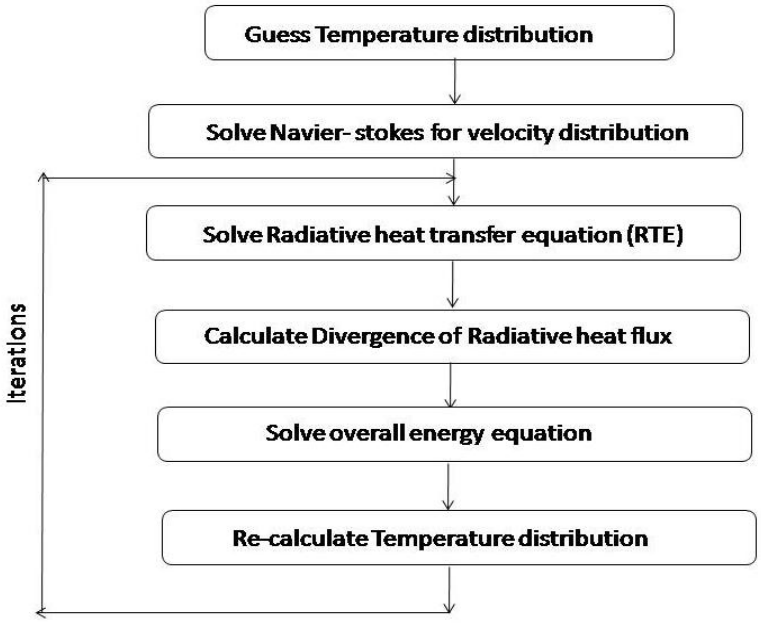

Fig. 3.17 flow chart of Solution algorithm

Above Fig. 3.17 shows the algorithm used to solve the system of equations. When applied to all of the flux and energy equations, the overall result of this process is a system of equation:

$$[A][X] = [B] \qquad (3.50)$$

For each of the two coordinate directions. The matrix [A] is a tri-diagonal matrix of coefficients depending on the local optical properties in the middle of the receiver, glass and walls. The vector [B] contains the temperature in the forward direction of receiver, which are assumed

Chapter 4

Results and Discussion

4.1 Introduction

In the present chapter, results of the simulations run on MATLAB and DDSCAT have been presented. In order to assess the candidature of various nanopaticle for their applicability in volumetric absorption solar thermal systems, it is imperative to study their optical characteristics in the solar irraiance wavelength band (0.3 μm to 2.5 μm). Furthermore, to quantify the absorption capability, solar weighted absorptivity of various nanoparticle dispersions have been computed. Essentially, the first part of this chapter deals with the determination of optical signatures of various nanoarticle dispersions (various size and shapes of copper nanoparticles dispersed in common heat transfer liquids). Finally, the most suitable nanoparticle-basefluid combination has been used as an input to calculate performance characteristics of nanofluid-based volumetric absorption solar thermal systems.

4.2 Suitable Nanoparticles-basefluid mix for solar thermal applications

In the present work, copper nanoparticles of various shapes such as sphere, spheroid and cube dispersed in water/silicone oil have been assessed. DDSCAT software which is based on DDA (discrete dipole approximation have employed for calculating the spectral absorption, scattering and extinction efficiencies defined by Eq. 4.1 - 4.3 respectively.

$$Q_{abs_\lambda} = \frac{C_{abs_\lambda}}{G}, \tag{4.1}$$

$$Q_{asca} = \frac{C_{sca_\lambda}}{G}, \tag{4.2}$$

$$Q_{ext_\lambda} = \frac{C_{ext_\lambda}}{G} \tag{4.3}$$

Where, C_{abs_λ}, C_{abs_λ}, and C_{abs_λ} are the absorption, scattering, extinction areas and G is the geometric projected area of the nanoparticle.

For the aforementioned calculations spectral size dependent complex refractive indices have been employed. These size dependent refractive indices have been calculated from their bulk values using the following equation:

$$\varepsilon(\omega,D)=\varepsilon(\omega)+\omega_p^2\left(\frac{1}{\omega^2+\Gamma_o^2}-\frac{1}{\omega^2+\Gamma_D^2}\right)+i\frac{\omega_p^2}{\omega}\left(\frac{\Gamma_D}{\omega^2+\Gamma_D^2}-\frac{\Gamma_o}{\omega^2+\Gamma_o^2}\right) \quad 4.4$$

Where, ω_p is the bulk Plasmon frequency, ω is the frequency of the electromagnetic wave, $\Gamma_o$is the bulk metal damping coefficient. It is this coefficient which is effectively modified in order to include size effects.

These spectral size dependent optical constants form the input to the DDSCAT. DDSCAT computes the spectral absorption and scattering efficiencies for the nanoparticle – base-fluid combination. Fig. 4.1 shows the optical signatures of cube shaped nanoparticles dispersed in silicone oil. The peaks of absorption and scattering efficiencies occur in the visible region. The magnitude of these peaks increases with increase in the particle size. Furthermore, absorption efficiencies are several times the corresponding scattering efficiencies depicting that nanoparticles are strong absorbers of electromagnetic radiations. The characteristic of the scattering efficiencies spectrum are mainly due to the size of particle, hence its spectra of nanocube decay slowly as the radius increases, i.e. the cube becomes larger it scatters light at longer wavelength.

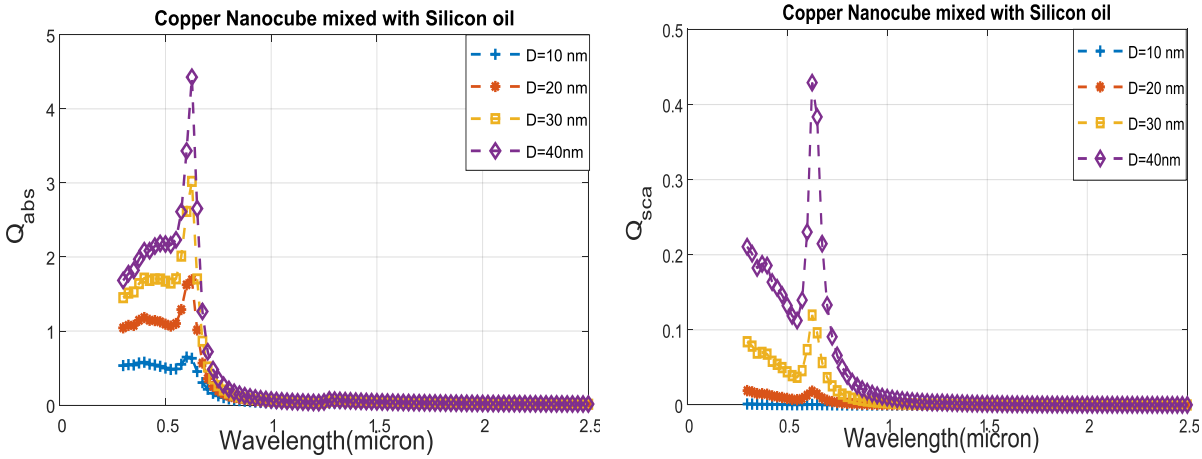

Fig. 4.1 Absorption (a) and scattering (b) coefficient of copper nanoparticles (cube shape) mixed with silicon oil

Figure 4.2 and 4.3 show the absorption and scattering efficiencies of copper nano-spheres dispersed in silicone oil and water. These follow similar trends as with the nano-cubes i.e. absorption efficiencies being several time their scattering efficiencies. Furthermore, a unique blue shift in the peaks is observed when the dielectric media is changed from silicone oil to water. The reflective index of medium affects both absorption and scattering efficiencies peaks magnitude, also shifts the peak towards infrared region. In scattering

efficiency two peaks are observed at D=40 nm, i.e. as the particle size become larger it deflects the high wavelength wave.

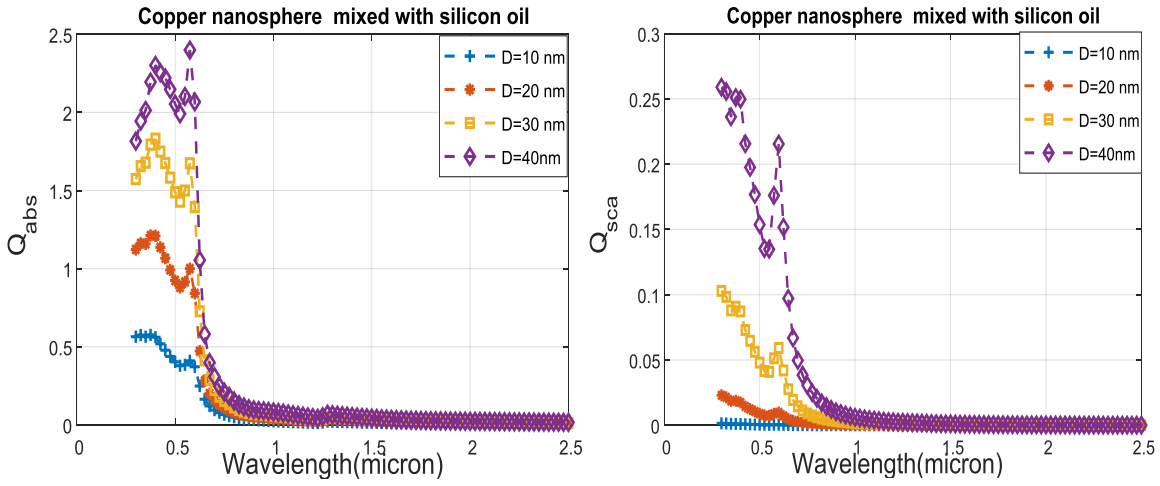

(a) (B)

Fig. 4.2 Absorption (a) and scattering (b) coefficient of copper nanoparticles (sphere shape) mixed with silicon oil

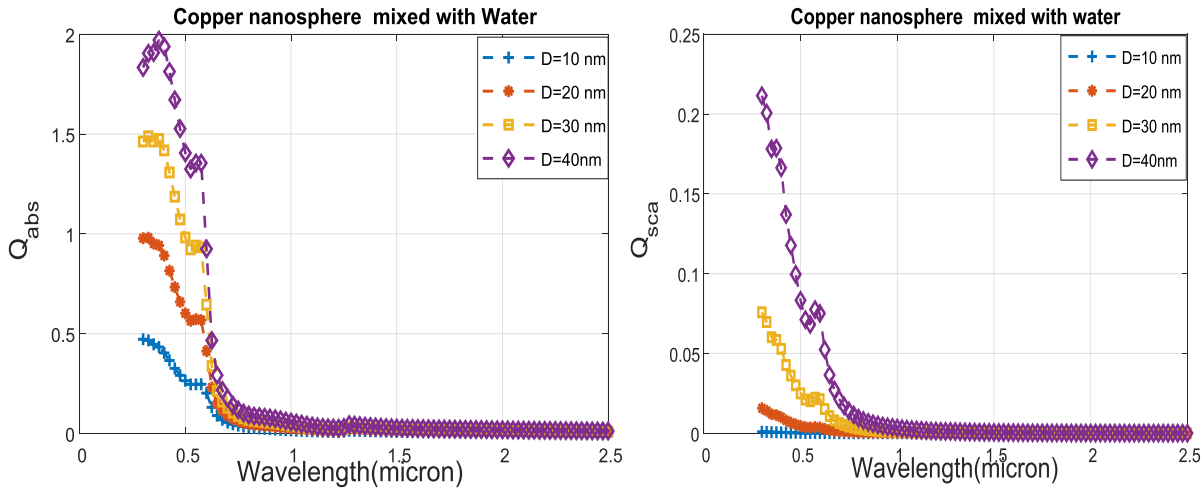

(a) (b)

Fig. 4.3 Absorption (a) and scattering (b) coefficient of copper nanoparticles (sphere shape) mixed with water

Optical signatures of copper nano-spheroids follow a unique trend (see Fig. 4.4). With the effective radius fixed if the aspect ratio of the nano-spheroid is altered there is marked shift in the absorption and scattering efficiency peaks. On the other hand, for a given aspect ratio the only the magnitude but not the location of these peaks change (see Fig. 4.5). This aspect in particular could be seminal in engineering nanoparticle dispersions which could have peaks across the solar irradiance wavelength band. In order to quantify the magnitude of

solar absorption capability a parameter called solar weighted absorption coefficient is defined and is given by Eq. 4.5 as

$$A_{swa} = \frac{\int_0^{2.5\mu m} E_\lambda \left(1 - e^{-K_{nd,\lambda} y}\right) d\lambda}{\int_0^{2.5\mu m} E_\lambda d\lambda} \qquad 4.5$$

Physically, this expression gives an idea of the fraction of the energy absorbed by given thickness of liquid column. Higher the value, better it is for solar thermal applications.

Fig.4.6 shows that solar weighted absorption coefficient increases with increase in volume fraction of the nanoparticles. The rate of increase being much higher for spheroid nanoparticles, depicting that shape could indeed be instrumental in dictating the solar weighted absorption coefficient.

Finally, the effect of basefluid on the optical signatures has been assessed. Everything else being same, if the same nanoparticles are dispersed in different base-fluids (having different index of refraction) different peak locations are observed. Specifically, with increase in the magnitude of index of refraction of the basefluid, there is a red shift (shift towards longer wavelengths) of the absorption efficiency peaks.

As a whole, it could be concluded that nanoparticle shape, size and the base fluid should be carefully chosen to ensure high solar irradiation absorption capability at low volume fractions.

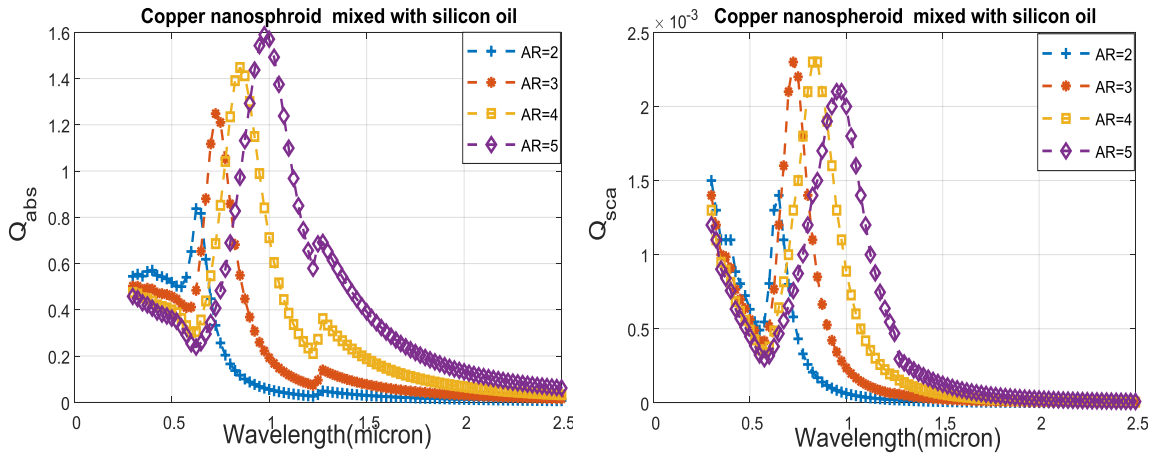

(a) (b)

Fig. 4.4 Absorption coefficients (a) and scattering coefficients (b) of copper nanoparticles (spheroid shape) mixed with silicon oil at Aspect Ratio 2, 3, 4 and 5

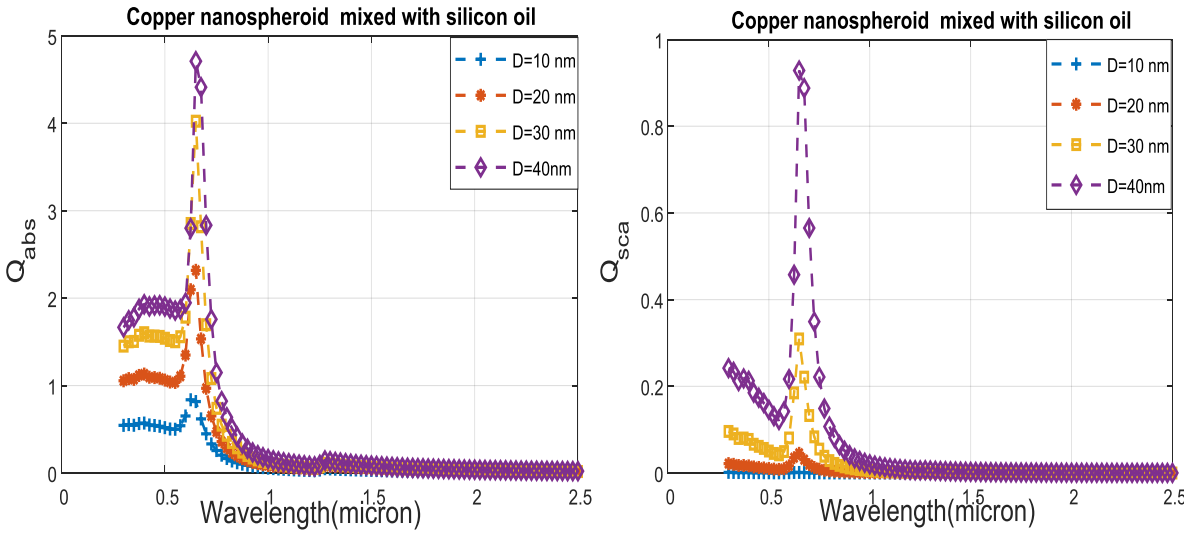

(a) (b)

Fig.4.5Absorption coefficients (a) and scattering coefficients (b) of cupper nanoparticles (spheroid shape) mixed with silicon oil at diameter 10 nm, 20 nm, 30 nm and 40 nm

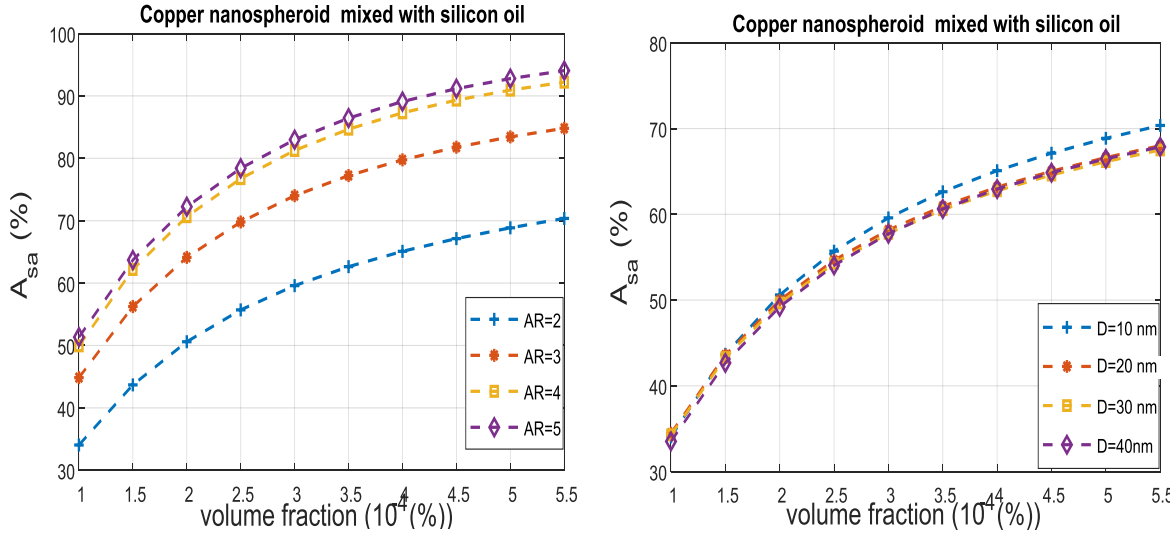

(a) (b)

Fig. 4.6 Solar weighted absorption coefficient for (a) different aspect ratios of *A* = 2, 3, 4, and 5 (b) different diameter of *D* = 10, 20, 30, and 40 nm of nanoparticles mixed with silicon oil as a function of volume fraction.

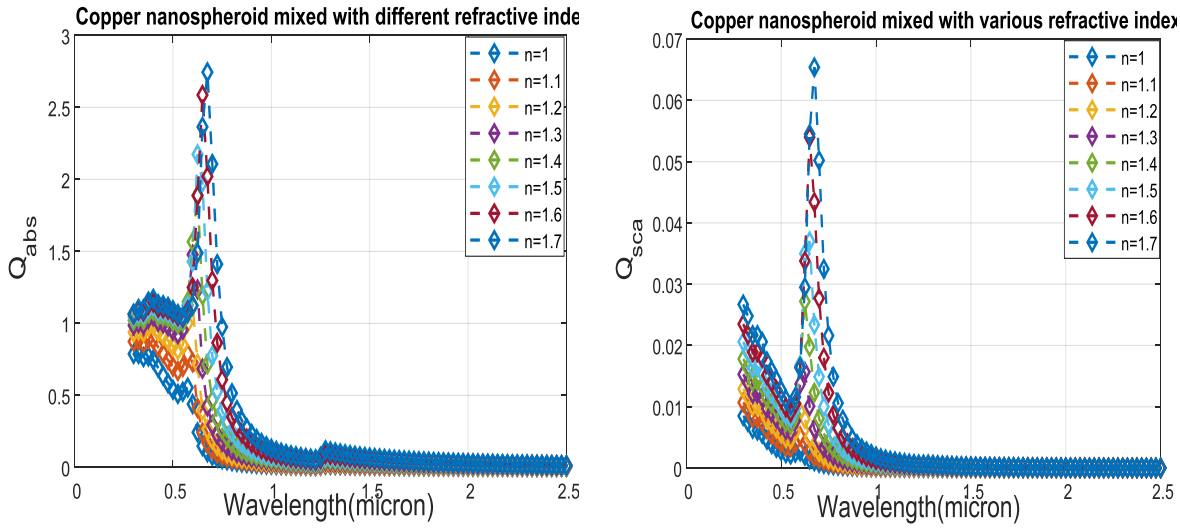

(a) (b)

Fig.4.7 Absorption coefficients (a) and scattering coefficients (b) of copper nanoparticles (spheroid shape) at various Reflective indexes

4.3 Effect of varying solar concentration factors

Figure 4.8 shows the effect of solar irradiation concentration on thermal efficiency and average outlet temperature as the inlet fluid temperature increases. With the same volume fraction of nanofluid 0.05%, receiver height 10 cm and bulk fluid inlet velocity is fixed by 1 mm/s, the inlet fluid temperature vary from 373 K to 573 K and solar concentration ratio varies from 10 to 50 undergoing to same expose time.

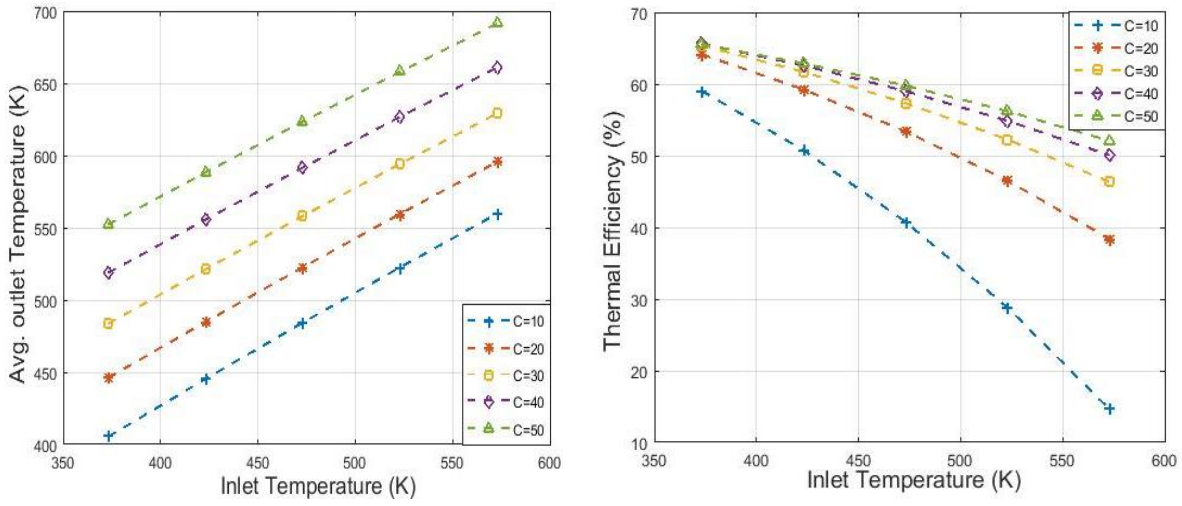

(a) (b)

Fig. 4.8 Effect of varying solar concentration with inlet fluid temperature (a) variation of average outlet fluid temperature (b) variation of thermal efficiency

Maximum average outlet temperature is obtained at higher solar concentration ratio, fig 4.8 (a) shows the effect of outlet average temperature, average outlet temperature increases linearly with the bulk inlet fluid temperature and increases with solar concentration. Highest outlet temperature implies the higher thermal efficiency of the volumetric receiver, as the bulk inlet temperature increase the thermal efficiency decay sharply due to radiative losses dominated at high temperature receiver application as shown in fig. 4.8 (b).

Figure 4.9 demonstrates the effects of sun concentration and bulk inlet fluid temperature over the convective and radiative losses of the receiver. Convective losses are the function of temperature difference between glass cover temperature and atmospheric temperature, hence at high concentration i.e. high top glass temperature, convective losses will be higher, also by increasing the bulk fluid inlet temperature convective losses increases sharply as shown in fig 4.9 (a). Similarly the radiative losses are the function of fluid inlet temperature and the solar concentration ratio, hence radiative losses increases as the bulk fluid inlet temperature increases and also by varying the solar concentration ratio as shown in Fig. 4.9 (b).

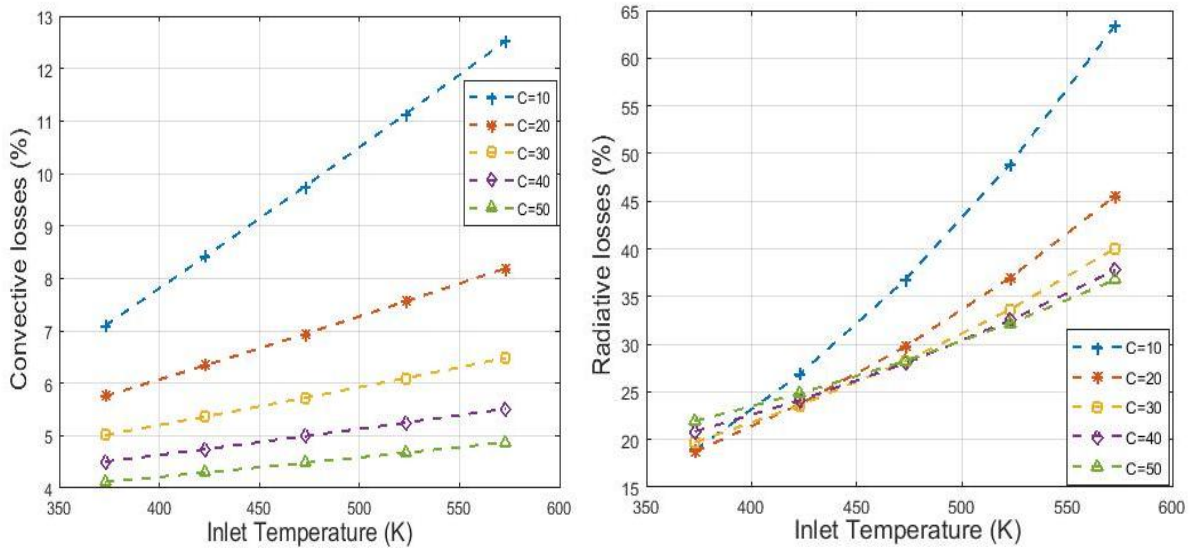

(a) (b)

Fig. 4.9 variation of (a) convective losses and (b) radiative losses with sun concentration and bulk fluid inlet temperature

4.4 Effect of varying optical properties of wall

As per the assumption of receiver modeling the bottom wall of the receiver is optically insulated, hence the wall can only absorbed and reflect the solar irradiation. Reflectivity of wall plays a significant role in the performance of the receiver as shown in fig. 4.10 and 4.11.

Thermal efficiency of the receiver at different reflective boundaries condition is shown as fig. 4.10 (a), from the graph it can be concluded that thermal efficiency will be higher when the reflectivity of wall be zero i.e. wall will absorbed all the incident solar irradiation, also decreases as the reflectivity of wall gradually increases. The effect of bulk fluid inlet temperature is gradually drop in thermal efficiency due to higher radiative losses occur from the receiver.

Figure 4.10 (b) shows the effect of outlet average fluid temperature as the reflectivity and bulk fluid inlet temperature varies. In similar fashion, the outlet average fluid temperature will be higher when the reflectivity of wall becomes zero, and increases with the bulk inlet fluid temperature.

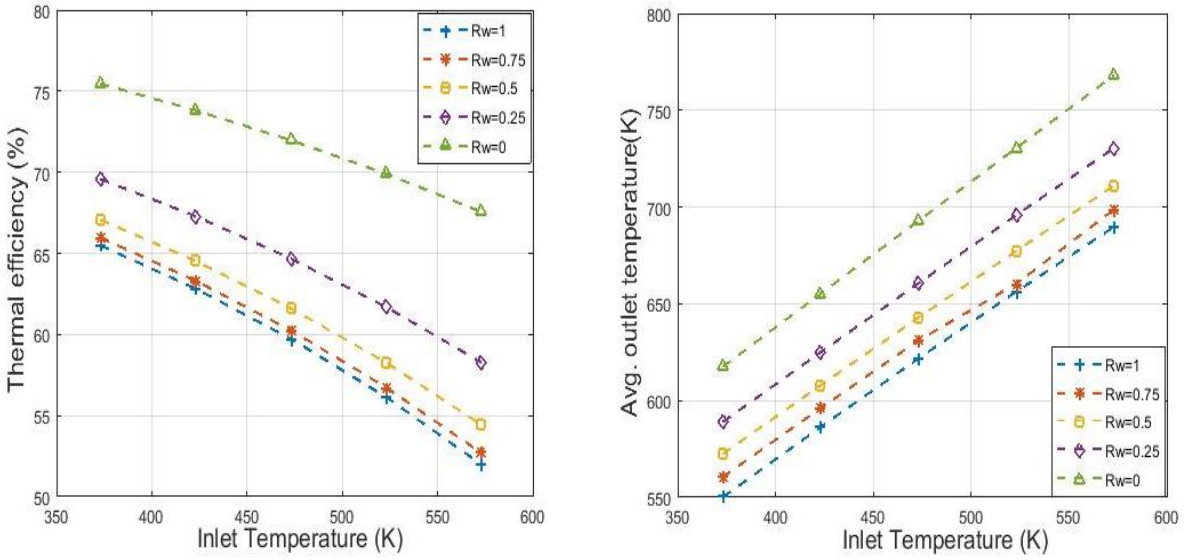

(a) (b)

Fig 4.10 variation of (a) thermal efficiency and (b) average outlet temperature with reflectivity of wall and bulk fluid inlet temperature

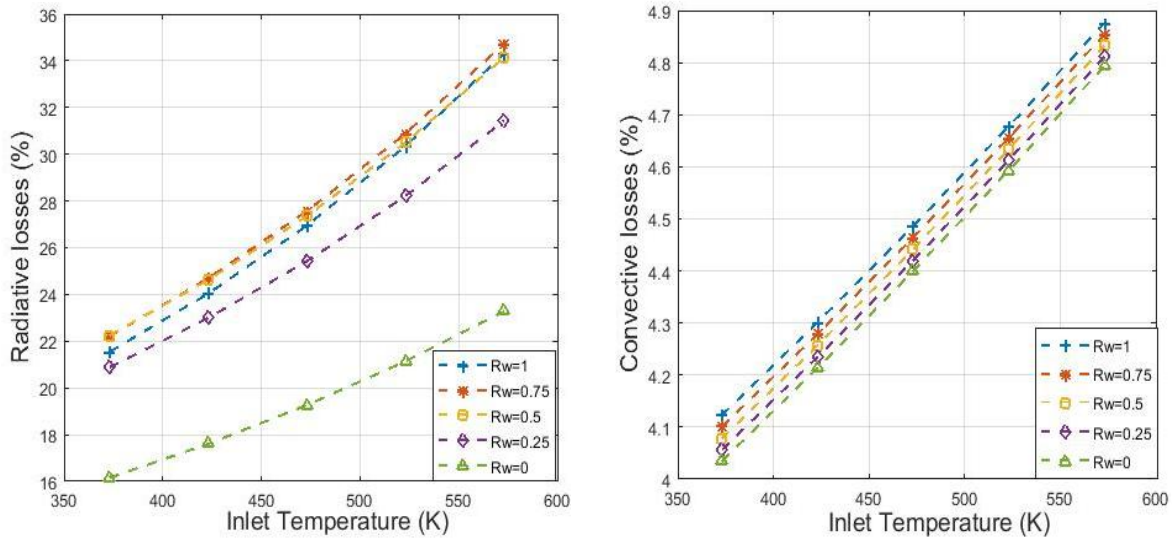

(a) (b)

Fig 4.11 variation of (a) Radiative losses and (b) Convective losses with reflectivity of wall and bulk fluid inlet temperature

Figure 4.11 (a) and (b) shows the variation of convective and radiative losses by varying reflectivity and bulk fluid inlet temperature. It can be concluded that, convective and radiative losses will be maximum when the wall become pure reflective and minimum when the wall become purely absorptive. Convective and radiative losses also vary with bulk fluid inlet temperature, i.e. at lower bulk fluid inlet temperature the convective and radiative losses will be lower and gradually increases by increasing the bulk fluid inlet temperature.

Chapter 5

Conclusion and Future work

5.1 Conclusion

In this thesis an innovative idea is proposed for collecting solar energy with the potential to increase thermal efficiency of concentrated solar power applications by using nanofluids as HTF inside the receiver. It is observed that the effect of design of solar collector receiver such as height, solar concentration, and optical properties of nanoparticles and boundary conditions of the receiver plays a significant role in the performance of the receiver.

Following paragraph briefly described the key conclusions from the present work

- Optical properties of nanoparticles closely related to shape, size and the medium in which the nanoparticles dispersed. As the aspect ratio of nanoparticles and effective diameter varies the absorption and scattering peaks of changes significantly, also solar weighted absorption coefficient increases with volume fraction of the nanoparticles.
- At higher solar concentration ratio, the thermal efficiency of the receiver and the average outlet fluid temperature will be higher, and the radiative and convective loss varies with bulk fluid inlet temperature.
- At purely absorbing bottom wall, the thermal efficiency of the receiver and the average outlet fluid temperature will be higher.

5.2 Future work

- The nanoparticles size effects quantity the solar weighted absorption coefficient; hence it is important to take account for the shape and size of nanoparticles in base fluid, also the reflective index of the base fluid enhance the absorption tendency of nanofluids.
- The boundaries of the receiver should be suitably selected. The height of the receiver is the important parameter which affects the overall thermal performance of the system.

Appendix A

The incident solar radiation flux is fall over the solar thermal receiver at normal direction. The glass cover at the top of the receiver allows the sun radiation to directly interact with nanofluids. The sun rays travel inside the receiver and deflected by the boundary of the system, i.e. multiple reflection, also the HTF inside the receiver absorbed the energy contain in sun rays. The intensity of this flux is reduces as it travel inside the receiver as shown in Figure A1.

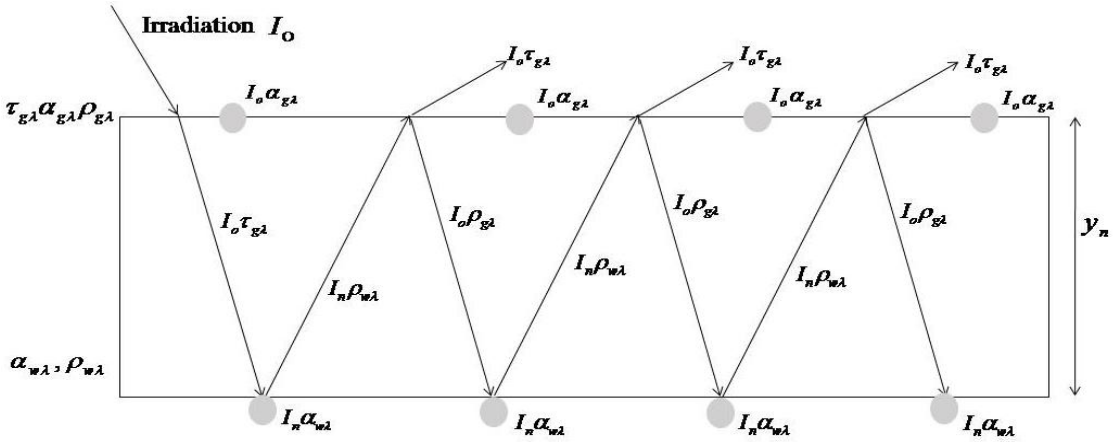

Fig. A1: Multiple reflection of solar radiation inside the receiver

The spectral absorption properties of glass cover absorbed the incident flux and transmitted it spectrally inside the receiver, intensity of flux decay as it travel through the HTF due to its spectral absorption characteristics. The intensity reaches the bottom surface again absorbed and reflected back to the receiver, again fluid absorbed the intensity and so on. The multiple reflection of intensity take place until it is totally absorbed and transmitted through the receiver.

Since the receiver discretized with finite difference method, the top and bottom node taken as half node, hence the total energy absorbed by the top and bottom node is listed as,

$$I_{store}^{top} = I_{\mathrm{O}}\left(1-\exp\left(-k_{a\lambda}\frac{dy}{2}\right)\right)\left\{1+\rho_w\rho_g\exp(-k_{a\lambda}2y_n)+\rho_w^2\rho_g^2\exp(-k_{a\lambda}4y_n)+\rho_w^3\rho_g^3\exp(-k_{a\lambda}6y_n).....\right\}$$
$$-I_{\mathrm{O}}\left(1-\exp\left(k_{a\lambda}\frac{dy}{2}\right)\right)\left\{\rho_w\exp(-k_{a\lambda}2y_n)+\rho_w^2\rho_g\exp(-k_{a\lambda}4y_n)+\rho_w^3\rho_g^2\exp(-k_{a\lambda}6y_n).....\right\} \quad (1\ \mathrm{A})$$

$$I_{store}^{bottom} = I_{\mathrm{O}}\left(\exp\left(k_{a\lambda}\frac{dy}{2}\right)-1\right)\exp(-k_{a\lambda}y_n)\left\{1+\rho_w\rho_g\exp(-k_{a\lambda}2y_n)+\rho_w^2\rho_g^2\exp(-k_{a\lambda}4y_n)+\rho_w^3\rho_g^3\exp(-k_{a\lambda}6y_n).....\right\}$$
$$+I_{\mathrm{O}}\left(1-\exp\left(-k_{a\lambda}\frac{dy}{2}\right)\right)\rho_w\exp(-k_{a\lambda}y_n)\left\{1+\rho_w\rho_g\exp(-k_{a\lambda}2y_n)+\rho_w^2\rho_g^2\exp(-k_{a\lambda}4y_n)+\rho_w^3\rho_g^3\exp(-k_{a\lambda}6y_n).....\right\}$$
(1 B)

The above Eq. 1A and 1B can be represents the geometric progression series form, which can be extended up to infinity. The above equation can also be written in summation of infinite G.P series, as listed below,

$$I_{store}^{top} = I_{\mathrm{O}}\left[\left(\exp\left(-k_{a\lambda}\frac{dy}{2}\right)-1\right)\rho_{w\lambda}\left(\frac{\exp(-k_{a\lambda}2y_n)}{1-\rho_w\rho_g\exp(-k_{a\lambda}2y_n)}\right)+\left(1-\exp\left(-k_{a\lambda}\frac{dy}{2}\right)\right)\rho_{w\lambda}\left(\frac{1}{1-\rho_w\rho_g\exp(-k_{a\lambda}2y_n)}\right)\right]$$
(2 A)

$$I_{store}^{bottom} = I_{\mathrm{O}}\left[\left(\exp\left(k_{a\lambda}\frac{dy}{2}\right)-1\right)\left(\frac{\exp(-k_{a\lambda}2y_n)}{1-\rho_w\rho_g\exp(-k_{a\lambda}2y_n)}\right)+\left(1-\exp\left(-k_{a\lambda}\frac{dy}{2}\right)\right)\rho_w\left(\frac{\exp(-k_{a\lambda}2y_n)}{1-\rho_w\rho_g\exp(-k_{a\lambda}2y_n)}\right)\right]$$
(2 B)

With the help of Eq. 2A and 2B, we can determine the sum of spectral energy absorbed in the top glass cover and bottom wall, which can be added with energy Eq. 3.45 and 3.47. Furthermore, the intensity absorbed by the interior nodes depends on the spectral optical thickness of the receiver; hence the spectral intensity absorbed by the interior node can be listed as,

$$I_{store}^{interior} = I_{\mathrm{O}}\left[\left(\exp\left(-k_{a\lambda}n\frac{dy}{2}\right)-\exp\left(-k_{a\lambda}(n+1)\frac{dy}{2}\right)\right)\left(\frac{1}{1-\rho_w\rho_g\exp(-k_{a\lambda}2y_n)}\right)-\left(\left(\exp\left(k_{a\lambda}n\frac{dy}{2}\right)-\exp\left(k_{a\lambda}(n+1)\frac{dy}{2}\right)\right)\right)\left(\frac{\exp(-k_{a\lambda}2y_n)}{1-\rho_w\rho_g\exp(-k_{a\lambda}2y_n)}\right)\right]$$
(3)

The Eq. 3 gives total sum of normal spectral intensity stored in middle nodes; here n represents the location of spectral domain. This equation can also be added to the energy Eq.3.49 for interior nodes.

Ones the reflected intensity back from wall reached to glass cover. The spectral absorption, reflection and transmission property of glass allows the intensity to propagate with their properties. The energy transmitted through the top glass cover, also referred as optical losses from receiver, is the sum of overall spectral intensity transmitted through glass cover in multiple reflections, which can be written as,

$$\text{Optical Loss}= \tau_{g\lambda}I_o\rho_w\left\{\exp(-k_{a\lambda}2y_n)+\rho_w\rho_{g\lambda}\exp(-k_{a\lambda}4y_n)+\rho_w^2\rho_{g\lambda}^2\exp(-k_{a\lambda}6y_n)+.....\infty\right\}$$
(4A)

Also Eq. 4A can be written as in form of infinite summation of G.P. series,

$$\text{Optical Loss} = \rho_w \tau_{g\lambda} I_o \left(\frac{\exp(-k_{a\lambda} 2y_n)}{1 - \rho_w \rho_g \exp(-k_{a\lambda} 2y_n)} \right) \quad (4B)$$

The Eq. 4 B gives the overall optical losses of the receiver. Along with optical losses glass absorb incident radiation spectrally from bottom of the receiver. Hence in similar fashion, the total amount of intensity absorbed by the glass can be calculated, which is given as

$$\text{Total absorb} = \rho_w \alpha_{g\lambda} I_o \left(\frac{\exp(-k_{a\lambda} 2y_n)}{1 - \rho_w \rho_g \exp(-k_{a\lambda} 2y_n)} \right) \quad (5)$$

Bibliography

Retrieved from http://www.energynext.in/indias-first-csp-plant-commissioned-under-jnnsm/

Bhalla, V., & Tyagi, H. (2017). Solar energy harvesting by cobalt oxide nanoparticles, a nanofluid absorption based system. *Sustainable Energy Technologies and Assessments.*

Bohren, C. F., & Huffman, D. R. (2008). *Absorption and scattering of light by small particles.* John Wiley & Sons.

Brewster, M. Q. (1992). *Thermal radiative transfer and properties.* John Wiley & Sons.

Chen, M., He, Y., Zhu, J., & Wen, D. (2016). Investigating the collector efficiency of silver nanofluids based direct absorption solar collectors. *Applied Energy,181* , 65-74.

Ghadimi, A., Saidur, R., Metselaar, & C., H. S. (2011). A review of nanofluid stability properties and characterization in stationary conditions. *International Journal of Heat and Mass Transfer, 54(17)* , 4051-4068.

Hordy, N., Rabilloud, D., Meunier, J. L., & Coulombe, S. (2014). High temperature and long-term stability of carbon nanotube nanofluids for direct absorption solar thermal collectors. *Solar Energy, 105* , 82-90.

Hwang, Y. J., Lee, J. K., Lee, C. H., Jung, Y. M., Cheong, S. I., Lee, C. G., et al. (2007). Stability and thermal conductivity characteristics of nanofluids. *Thermochimica Acta, 455(1)* , 70-74.

Kaluri, R., Vijayaraghavan, S., & Ganapathisubbu, S. (2015). Model Development and Performance Studies of a Concentrating Direct Absorption Solar Collector. *Journal of Solar Energy Engineering, 137(2)* , 021005.

Khullar, V., & Tyagi, H. (2010). Application of nanofluids as the working fluid in concentrating parabolic solar collectors. *37th National & 4th International Conference on Fluid Mechanics & Fluid Power, IIT Madras, Chennai, India,*, (pp. 16-18).

Khullar, V., Bhalla, V., & Tyagi, H. (2017). *Potential Heat Transfer Fluids (Nanofluids) for Direct Volumetric Absorption-Based Solar Thermal Systems,Journal of Thermal Science and Engineering Applications.*

Khullar, V., Tyagi, H., Phelan, P. E., Otanicar, T. P., Singh, H., & Taylor, R. A. (2012). Solar energy harvesting using nanofluids-based concentrating solar collector. *Journal of Nanotechnology in Engineering and Medicine, 3(3),* , 031003.

Kim, H. J., Bang, I. C., & Onoe, J. (2009). Characteristic stability of bare Au-water nanofluids fabricated by pulsed laser ablation in liquids. *Optics and Lasers in Engineering, 47(5),* , 532-538.

Lenert, A., & Wang, E. N. (2012). Optimization of nanofluid volumetric receivers for solar thermal energy conversion. *Solar Energy, 86(1),* , 253-265.

Lewis, N. S. (2007). Toward cost-effective solar energy use. *Secience 315, no 5831* , 798-801.

Liu, J., Ye, Z., Zhang, L., Fang, X., & Zhang, Z. (2015). A combined numerical and experimental study on graphene/ionic liquid nanofluid based direct absorption solar collector. *Solar Energy Materials and Solar Cells, 136,* , 177-186.

Luo, Z. W., C., W. W., Xiao, G., & Ni, M. (2014). Performance improvement of a nanofluid solar collector based on direct absorption collection (DAC) concepts. *International Journal of Heat and Mass Transfer* , 262-271.

MINARD, J. E., & CHUANG, H. N. (1974). PERFORMANCE OF A "BLACK" LIQUID FLAT-PLATE SOLAR COLLECTOR. *Solar Energy volume-17* , 179-183.

Otanicar, T. P., Phelan, P. E., Prasher, R. S., Gary, R., & Taylor, a. R. (2010). Nanofluid-based direct absorption solar collector. *Journal of renewable and sustainable energy 2* , 033102.

Otanicar, T., Taylor, R. A., Phelan, P. E., & & Prasher, R. (2009). Impact of size and scattering mode on the optimal solar absorbing nanofluid. *In Proceedings of the ASME 2009 3rd International Conference of Energy Sustainability, ASME,* (pp. pp. 791-796). San Francisco: CA.

Prasher, R. S., & Phelan, P. E. (2005). Modeling of radiative and optical behavior of nanofluids based on multiple and dependent scattering theories. *Paper No. IMECE2005-80302, ASME IMECE,.* Orlando, FL.

Rubin, M. (1985). Optical properties of soda lime silica glasses. *Solar energy materials, 12(4),* , 275-285.

SousaLd. Energy vision 2050. (2008). Retrieved from http://europe.theoildrum.com/node/4485

Taylor, R. A., Phelan, P. E., Todd, P. O., Chad, A. W., Nguyen, M., Trimble, S., et al. (2011). Applicability of nanofluids in high flux solar collectors. *Journal of Renewable and Sustainable Energy 3* .

Taylor, R., Coulombe, S., Otanicar, T., Phelan, P., Gunawan, A., Lv, W., et al. (2013). Small particles, big impacts: a review of the diverse applications of nanofluids. *Journal of Applied Physics* , 113(1), 1.

Tyagi, H., Phelan, P., & Ravi, P. (2009). Predicted efficiency of a low-temperature nanofluid-based direct absorption solar collector. *Journal of solar energy engineering 131* , 041004.

Veeraragavan, A., Lenert, A., Yilbas, B., Al-Dini, S., & Wang, E. N. (2012). Analytical model for the design of volumetric solar flow receivers. *International Journal of Heat and Mass Transfer* , 556-564.

Wei, X., & Wang, L. (2010). Synthesis and thermal conductivity of microfluidic copper nanofluids. *Particuology, 8(3)* , 262-271.

Yousefi, T., Shojaeizadeh, E., Veysi, F., & Zinadini, S. (2012). An experimental investigation on the effect of pH variation of MWCNT–H 2 O nanofluid on the efficiency of a flat-plate solar collector. *Solar energy* , 771-779.